SCIENCE CHINA
Information Sciences

• REVIEW •

September 2026, Vol. 69, Iss. 9, 191401:1–191401:18
https://doi.org/10.1007/s11432-025-4789-2

Integration of two-dimensional magnets in magnetic tunnel junctions: prospects and challenges

Qiuqiu LI[1], Kun HE[2*], Ruirui NIU[3], Ruixia WU[4], Jia LI[5], Bo LI[3*] & Xidong DUAN[5*]

[1]*College of Materials Science and Engineering, Changsha University of Science & Technology, Changsha 410114, China*
[2]*School of Physics and Optoelectronics, Xiangtan University, Xiangtan 411105, China*
[3]*National Key Laboratory of Power Semiconductor and Integration Technology, Engineering Research Center of Advanced Semiconductor Technology and Application of Ministry of Education, College of Semiconductors (College of Integrated Circuits), Hunan University, Changsha 410082, China*
[4]*School of Physics and Electronics, Hunan University, Changsha 410082, China*
[5]*State Key Laboratory of Chemo and Biosensing, Hunan Provincial Key Laboratory of Two-Dimensional Materials, College of Chemistry and Chemical Engineering, Hunan University, Changsha 410082, China*

Received 30 October 2025/Revised 8 December 2025/Accepted 4 February 2026/Published online 13 August 2026

Abstract Magnetic memory technology continues to drive progress in non-volatile data storage, offering significant advantages in data retention and operational endurance. As a key component in memory architectures, the magnetic tunnel junction (MTJ) plays a central role in the development of modern spintronics by leveraging its bistable resistance states. The emergence of two-dimensional (2D) magnetic materials has further accelerated the advancement of high-performance MTJs, capitalizing on their exceptional magnetic properties and ideal van der Waals interfaces. This review begins by introducing 2D magnetic materials with diverse properties, encompassing both layered and non-layered structures. It then summarizes novel magnetic tunnel junctions engineered from these 2D materials. Next, the review outlines recent applications and progress in theoretical calculations pertinent to 2D magnetic tunnel junctions. Finally, it discusses future opportunities for employing 2D magnetic materials in the design of innovative MTJs for next-generation high-performance electronics.

Keywords 2D magnetic materials, magnetic tunnel junction, quantum tunneling, spintronics, magnetic random-access memory

Citation Li Q Q, He K, Niu R R, et al. Integration of two-dimensional magnets in magnetic tunnel junctions: prospects and challenges. Sci China Inf Sci, 2026, 69(9): 191401, https://doi.org/10.1007/s11432-025-4789-2

1 Introduction

Leveraging the intrinsic spin of electrons in magnetic materials offers a promising and efficient avenue for encoding and storing binary information in memory circuits. Compared to traditional charge-based storage technologies, spintronic devices exhibit superior non-volatile memory performance and static power efficiency. This advantage stems from the thermodynamic stability of spin-up and spin-down states, which enables persistent data retention with minimal energy dissipation [1]. The introduction of the giant magnetoresistance (GMR) effect in the 1980s marked a pivotal advancement for spin storage, write and readout, accelerating the development of modern spintronics [2]. The GMR effect allows the conversion of electronic spin information into a measurable resistance signal through a spin valve, highlighting its inherent compatibility with integrated circuit fabrication. Moreover, the pronounced tunnel magnetoresistance (TMR) effect exhibited in magnetic tunnel junctions (MTJs) has become a cornerstone of modern spintronics, enabling a higher magnetoresistance ratio [3, 4]. After decades of development, TMR ratios have reached up to 604%, far exceeding the 150% room-temperature magnetoresistance threshold required for commercial magnetic random-access memory (MRAM) [5]. The integration of MTJs as spin detection structures in MRAM has shown considerable reliability and scalability, exemplified by a 64-kb MRAM array in 2025 [6].

A typical MTJ consists of two ferromagnetic layers: a free layer (FL) and a reference layer (RL). The magnetization of the FL can be manipulated via spin-transfer torque (STT) or spin-orbit torque (SOT) effect, whereas the RL maintains a fixed magnetization state. These two ferromagnetic layers are separated by an insulating intermediate layer, facilitating efficient spin injection via quantum tunneling [7]. The commercialization of MRAM for solid-state drives has been facilitated by key breakthroughs in MTJ technology, including interfacial perpendicular magnetic anisotropy (PMA), the development of synthetic antiferromagnets (SAFs), and enhanced process

* Corresponding author (email: hekun@hnu.edu.cn, boli@hnu.edu.cn, xidongduan@hnu.edu.cn)

compatibility [8–10]. The commercialization of MRAM is underpinned by the sophisticated stacking of dozens of ultra-thin films [6, 10]. The precise stacking of adjacent thin films is strictly governed by lattice matching requirements [7]. This adherence to epitaxial principles is crucial for enhancing the crystallinity of these nanometer-thick films, thereby contributing to the formation of specific device architectures. The rigidity of the device architecture design imposes significant limitations on advancements in power consumption, performance parameters, and device yield [6, 8]. Furthermore, the approximate 20-nm limit of the MTJ feature size for these thin film materials imposes a significant constraint, making it difficult to meet the demand for increased device density [11]. Therefore, developing novel materials is crucial for enabling MTJ miniaturization and performance improvement to meet the evolving demands of semiconductor technology nodes.

Two-dimensional (2D) materials, particularly 2D magnetic materials, provide a versatile platform for advanced spintronic applications. Their intrinsic long-range atomic order ensures periodic magnetic structure even at the monolayer limit [12, 13]. The broad family of 2D magnets provides considerable design flexibility for spintronic device fabrication, and most exhibit an out-of-plane magnetic easy axis, making them highly suitable for spin device miniaturization [13–17]. Some 2D magnetic materials also possess high spin polarization—for instance, Fe_3GaTe_2 exhibits 80% spin polarization—enabling efficient generation of spin-polarized currents [18]. Van der Waals (vdW) stacking magnetic heterostructures enable the fabrication of atomically sharp interfaces free from chemical bonding, bypassing lattice-matching constraints and improving spin transport. 2D magnetic materials integrate seamlessly with conventional thin-film technologies, supporting the development of high-performance spintronic devices [19,20]. Therefore, 2D magnetic materials have attracted extensive attention in recent years due to their significant potential for applications in future magnetic storage devices, magnetic sensors, and spin-based logic devices.

This review presents a concise overview of recent advances, identifies emerging challenges, and discusses future opportunities related to the integration of 2D magnetic materials into MTJs. We begin by underscoring the fundamental role of MTJs in advancing spintronic memory technologies and their practical implementations. Next, we systematically survey reported 2D magnetic materials and highlight their successful integration into MTJs and other quantum-tunneling-based spintronic architectures. We then explore the unique advantages offered by 2D magnets within MTJs, supported by theoretical insights, and demonstrate their capacity to achieve well-defined resistance states. Finally, we outline future prospects for 2D material-based MTJ devices.

2 MTJs: the core of MRAM technology

In an MTJ, a tunneling layer with high crystal quality ensures coherent tunneling, which preserves the spin-polarized states during quantum tunneling, thereby enabling efficient spin injection into another ferromagnetic layer [21, 22]. Moreover, a pronounced spin-filter effect has been observed in high-quality tunneling layers, particularly in Fe/MgO/Fe architectures, leading to significantly enhanced current spin polarization [23]. The fundamental working principle of MTJ is based on the tunneling effect of spin-polarized electrons, which was first theoretically described by Mott's two-channel model in 1936 [24]. This model treats conduction electrons as two independent spin channels—spin-up and spin-down—each contributing separately to electron transport.

When the magnetization directions of the two ferromagnetic layers are parallel, electrons whose spin orientation is aligned with the magnetization direction experience less scattering when traversing the layers, forming a low-resistance conduction channel (Figure 1(a)). In this case, the efficient injection of majority spins from the FL into the RL results in a low-resistance state (R_P) of the device. Conversely, when the magnetizations are antiparallel, electrons preserve their spin orientation after passing through the first ferromagnetic layer but encounter strong spin-dependent scattering at the second layer due to its opposite magnetization direction (Figure 1(b)). In particular, the injection of majority spins from the FL into the minority spin orbitals of the RL impedes the efficient transport of spin-polarized electrons, leading to a high-resistance state (R_{AP}). This significant resistance difference ($R_{AP} > R_P$) directly reflects the TMR effect, which can be quantitatively characterized by the TMR ratio:

$$\mathrm{TMR} = \frac{R_{AP} - R_P}{R_P} \times 100\%. \tag{1}$$

In MTJs, the resistance-area product (RA)—defined as the product of junction resistance (R) and cross-sectional area (A)—serves as a key performance parameter. For MRAM applications, achieving low operating resistance is essential not only to fulfill the demands of low-power electronics but also to improve data readout speed. Given the structural dependence of MTJ resistance in multilayer stacks, RA is judiciously adopted as the primary evaluation metric. This parameter effectively normalizes the device resistance, thereby eliminating confounding geometric influences [25].

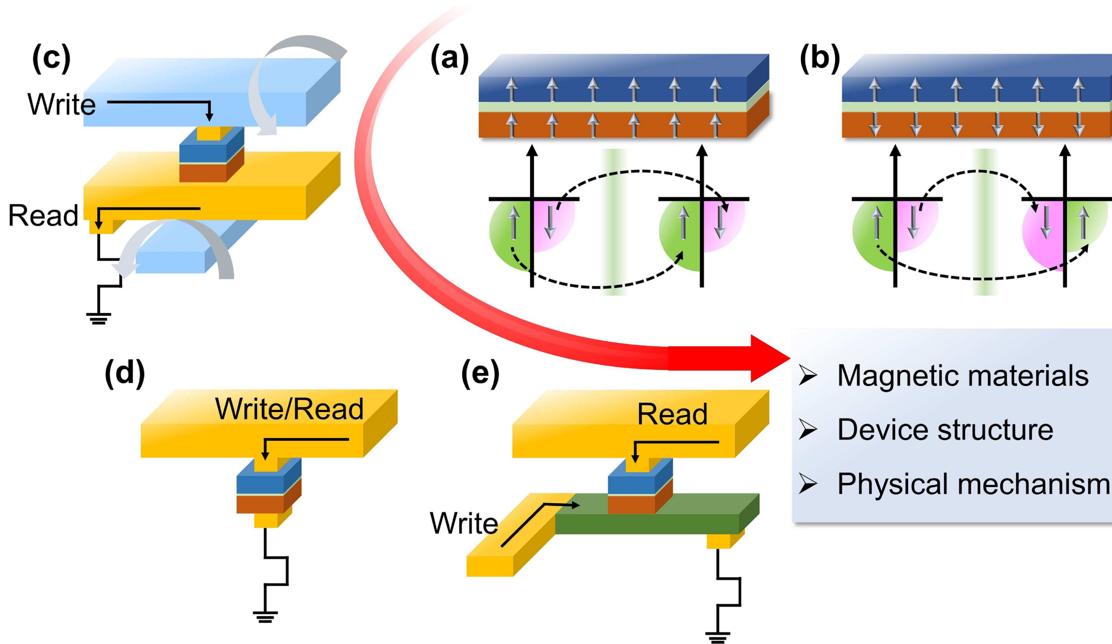

Figure 1 (Color online) The operating mechanism of MTJ and its integration in MRAM technology. Schematic diagram of an MTJ in (a) parallel and (b) antiparallel configuration. A chronological overview of MRAM development, spanning (c) Toggle-MRAM, (d) STT-MRAM, and (e) SOT-MRAM, wherein the MTJ functions as the critical readout element, supported by continuous optimization of writing techniques.

The distinct resistance states arising from parallel and antiparallel magnetization configurations enable MTJs to serve as fundamental building blocks in memory chips. MTJs act as the core reading element in MRAM, while writing techniques continue to evolve. The mechanism for switching the magnetization of the FL has progressed significantly, transitioning from Toggle-MRAM (Figure 1(c)), to STT-MRAM (Figure 1(d)), and more recently to SOT-MRAM (Figure 1(e)) [26]. In Toggle-MRAM, the magnetization reversal is realized using current-induced field through orthogonal bit and word lines [27]. This field-driven approach requires high write currents, leading to substantial power consumption and necessitating complex peripheral circuitry. Subsequently, the STT effect presents a compelling method for achieving FL magnetization reversal within the MTJ structure [28]. This mechanism relies on the transfer of spin angular momentum from a polarized current to the free layer, with the current direction determining the final magnetic state. Although STT-MRAM supports device scaling, its use of high writing currents and shared read/write path raises reliability concerns and limits endurance. In contrast, SOT-MRAM decouples the read and write paths through spin accumulation at ferromagnetic/non-magnetic interfaces, significantly improving device longevity. The spin Hall effect in heavy metals and the Rashba-Edelstein effect at interfaces facilitate current-induced spin accumulation, enabling efficient manipulation of the FL's magnetization [29, 30]. Owing to their high operating speed and integration density, MRAMs are promising candidates to replace conventional charge-based memories across various cache levels, from level 1 (cache) to level 4 (main memory) in the memory hierarchy [31]. They also offer compelling advantages for embedded non-volatile in-memory computing, outperforming existing RAM technologies in several aspects [32].

However, several challenges still need to be resolved to enable large-scale integration of MRAM into mainstream high-density integrated circuits. Firstly, despite the fabrication of numerous high-capacity embedded MRAM chips, maintaining competitiveness at advanced technology nodes necessitates stringent downscaling, particularly concerning MTJ diameter and cell-to-cell pitch [33]. Currently, the complexity and substantial thickness ($\sim$20 nm) of MTJ stacks pose significant challenges to ion-beam etching processes, inherently limiting attainable MTJ feature sizes to around 20 nm [11, 33]. Secondly, driving the broad commercial adoption of MRAM necessitates substantial improvements in TMR ratios. Even though reported room-temperature TMR values of 604% meet the criteria for magnetic sensors, a greater on-off ratio is essential to fulfill the performance requirements of digital Boolean logic [5]. Thirdly, a significant challenge lies in improving MTJ stacks and their versatility using conventional materials and integration processes [11]. These intricate stacks are comprised of dozens of ultrathin layers, where the precise characteristics of each material and interface critically influence overall device performance and micro-device fabrication. Additionally, the comprehensive optimization in write and read consumption, manufacturing cost, device yield, read and write speeds and thermal stability for MRAM should also be addressed. Therefore, continued research and innovation in magnetic materials, device architecture, and physical mechanisms are imperative to advance MRAM technology toward commercial adoption in high-performance memory and logic applications.

The enhancement of MRAM performance parameters, along with improved fabrication yield and integrated density, is critical to the commercial viability and market penetration. Requirements for PMA magnets and strict lattice-matching in epitaxial growth have largely standardized MTJ structures for conventional thin-film materials, with the CoFeB/MgO/CoFeB stack being a prominent example. Nevertheless, progress in material science is diversifying MTJ designs and boosting device performance. Among emerging materials, 2D magnetic materials are regarded as highly promising candidates due to their robust PMA and stable magnetic order at the atomic scale. Their introduction not only broadens the selection of magnetic materials but also unveils new device architectures and quantum tunneling phenomena in spin-polarized electron transport.

3 2D magnetic materials

Since the groundbreaking discovery of intrinsic long-range ferromagnetism in monolayer CrI_3 and bilayer $Cr_2Ge_2Te_6$ in 2017, the field of 2D magnetic materials has experienced rapid growth [12, 13]. Such a magnetic order has since been confirmed in numerous other 2D material platforms [34, 35]. 2D magnetic materials can be classified into two categories based on their structural characteristics: layered and non-layered (Figure 2). We employ 2D layered materials, Fe_3GeTe_2 and CrI_3, as illustrative examples to elucidate their distinct magnetic properties. In 2D Fe_3GeTe_2, the magnetic moments localized within the atomic orbitals of Fe atoms contribute to the emergence of macroscopic magnetism, characterized by a ferromagnetic spin ordering where adjacent Fe atoms exhibit parallel spin alignment (Figure 2(a)) [14]. Conversely, 2D CrI_3 exhibits an antiferromagnetic spin arrangement, featuring parallel spin orientation within a single layer and antiparallel orientation between adjacent layers (Figure 2(b)) [36]. Layered 2D magnetic materials exhibit a typical vdW crystal structure, where atoms within each layer are covalently bonded, while adjacent layers are bound by weak vdW forces, resulting in surfaces free of dangling bonds. This structural feature enables materials such as CrI_3, Fe_3GeTe_2, and $FePS_3$ to be readily exfoliated into atomically thin layers through mechanical exfoliation [12, 14, 37]. Figure 2(c) provides an overview of the atomic arrangement characteristics of commonly reported 2D layered magnetic materials.

In contrast, non-layered 2D magnetic materials are covalently bonded both within and between layers, but with a marked difference in bond strength: interlayer bonds are relatively weaker, whereas intralayer bonds are stronger. This bonding configuration generally precludes mechanical exfoliation, making epitaxial growth techniques such as chemical vapor deposition (CVD) necessary. For instance, the family of 2D Cr_xTe_y materials can be conceptualized as arising from the self-intercalation of Cr atoms within the $CrTe_2$ parent lattice, with a ratio of intercalated Cr to Cr within the backbone ranging from 0 to 1 (Figure 2(d)) [38]. The magnetic characteristics of these 2D Cr_xTe_y compounds are primarily governed by a combination of antiferromagnetic Cr-Cr direct exchange interactions and ferromagnetic superexchange interactions occurring within the Cr-Te-Cr units [39]. Critically, the spatial separation between neighboring Cr cations is sufficiently large, necessitating the mediation of spin alignment through a common Te anion to achieve an energetically favorable parallel arrangement. The interstitial insertion of Cr atoms inevitably perturbs their local atomic environment and exchange reaction with neighboring Cr atoms. Due to the significant spatial separation between intercalated Cr atoms and those within the backbone, the intercalated Cr is expected to induce spin canting [38, 39]. Nevertheless, the predominant out-of-plane magnetic easy axis and typically observed in the 2D Cr_xTe_y family indicates that the influence of intercalated Cr on the overall magnetic anisotropy is limited. Figure 2(e) illustrates the atomic arrangement characteristics of commonly reported 2D non-layered magnetic materials, thereby providing insights into their crystalline structures.

It is important to emphasize that 2D non-layered magnetic materials fundamentally differ from conventional magnetic thin films. First, they maintain long-range atomic order even at ultrathin thicknesses, preserving their intrinsic properties and providing an ideal platform for micro-nano spintronic design and explorations in theoretical physics. Second, they retain strong PMA down to atomic-scale thicknesses, with magnetic properties that are highly thickness-dependent. Third, they can be fully transferred onto other 2D materials to form high-quality vdW heterostructures with clean interfaces, offering an ideal system for investigating novel physical phenomena and developing functional devices. Compared to conventional magnetic thin films, 2D magnetic materials provide a broader range of material types, superior crystalline quality, and reduced lattice-matching constraints for magnetic heterostructure integration. As such, they are considered promising candidates for future memory technologies [15]. 2D non-layered magnetic materials significantly broaden the scope of material systems for both fundamental research and technological applications. More importantly, they serve as a crucial platform for constructing novel topological magnetic structures and precisely controlling chemical doping, thus facilitating favorable integration with non-

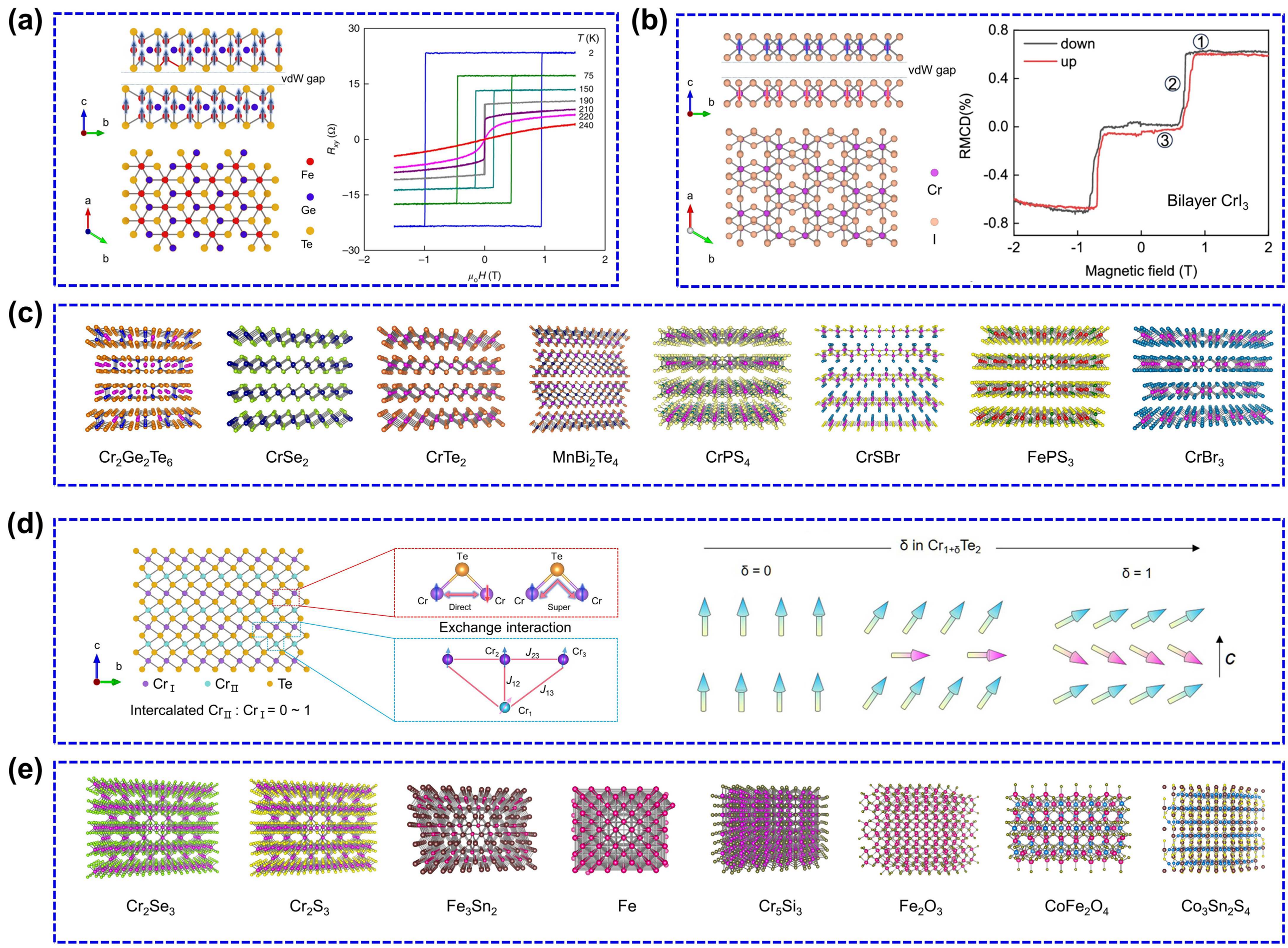

Figure 2 (Color online) 2D magnetic materials with layered and non-layered structures. Crystalline structure and magnetic properties of layered 2D (a) Fe_3GeTe_2 and (b) CrI_3 [14, 36] Copyright 2018 and 2024 Springer Nature; (c) drystalline structure of reported 2D magnetic materials with layered structures; (d) crystalline structure and magnetic properties of 2D chromium tellurides [38] Copyright 2020 American Physical Society; (e) crystalline structure of reported 2D magnetic materials with non-layered structures.

layered substrates for advanced device fabrication [16, 40].

2D magnetic materials host a rich variety of magnetic ground states, including ferromagnetism, antiferromagnetism, ferrimagnetism, and topological spin textures. Most 2D ferromagnetic materials exhibit strong magnetic anisotropy in the ultrathin limit, encompassing both in-plane and out-of-plane easy magnetization axes. The majority, including Fe_3GeTe_2 [14, 41], Fe_3GaTe_2 [15], Fe_3Sn_2 [42], $Cr_2Ge_2Te_6$ [13, 43, 44], $CrSe_2$ [45], $CrSiTe_3$ [46], exhibit out-of-plane easy axes, while a minority, such as 1T-$CrTe_2$ nanosheets (thicknesses >10 nm) [45], display in-plane anisotropy. Notably, 2D Fe_3GaTe_2 exhibits a high PMA energy density of approximately 4.17×10^5–4.79×10^5 J/m^3, surpassing that of conventional CoFeB films (2.1×10^5 J/m^3) [8, 15, 47].

Similarly, 2D antiferromagnetic materials comprise a diverse family, including CrX_3 (X = Cl, Br, I) [12,48–52] and transition metal phosphorous trichalcogenides (MPX_3, M = Mn, Fe, Ni; X = S, Se) [37,53–56]. Their intrinsic spin configuration can be either in-plane or out-of-plane, adapting to specific environmental requirements. The magnetic order in 2D antiferromagnets is considerably more complex than in their ferromagnetic counterparts, manifesting in various spin arrangements such as zigzag-type order in $NiPS_3$ [53, 54], $FePS_3$ [37] and $FePSe_3$ [57, 58]; A-type order in CrX_3 [12, 48–52]; and Néel-type order in $MnPS_3$ and $MnPSe_3$ [55, 56]. Beyond collinear structures, non-collinear antiferromagnetic configurations—where magnetic moments are oriented at an angle rather than strictly parallel or antiparallel—have also been observed, as in 2D Cr_5Si_3 nanosheets [59], resulting in a net magnetic moment.

Other magnetic configurations include ferrimagnetism, as seen in 2D ε-Fe_2O_3 [60], where antiparallel magnetic moments of unequal magnitude lead to a net uncompensated moment. This blend of ferromagnetic and antiferromagnetic traits makes ferrimagnetic materials attractive for applications in hard disk drives and magnetic transformers [61]. Certain local spin arrangements can also give rise to topologically non-trivial spin textures such as skyrmions [16, 62, 63], vortices [64], merons [65] and others [66]. Skyrmions, in particular, have been observed in a wide range of 2D magnets, including composite skyrmions in $Fe_{3-x}GeTe_2$ [67], Néel-skyrmions in Fe_3GaTe_2 [63], Bloch-type skyrmions in Fe_3GeTe_2 [68], and biskyrmions in Cr_3Te_4 [16]. Their stability is often attributed to the competition between the Dzyaloshinskii-Moriya interaction (DMI) and Heisenberg exchange coupling [69]. Though in systems with weak DMI, a balance among uniaxial anisotropy, dipolar interactions, and exchange coupling may also suffice [68,70–72]. Other emergent magnetic structures, such as the alternating spin texture in antiferromagnetic $MnTe_2$ [73], are also under active investigation.

A variety of advanced experimental techniques are employed to characterize the magnetic properties of 2D materials. (1) Raman spectroscopy probes magnon modes via spin-phonon coupling. Magnetic phase transitions can be identified through Raman mode splitting or shifts, as demonstrated in $Cr_2Ge_2Te_6$ [74]. (2) Photoluminescence (PL) spectroscopy responds to circularly polarized light under different magnetic states. For example, circularly polarized PL in $CrCl_3$ distinguishes magnetic arrangements in its monolayer and bilayer structures. Specifically, this technique reveals an antiferromagnetic interlayer interaction in the bilayer and a ferromagnetic arrangement within the monolayer [75]. (3) Magneto-optical effect, such as the magneto-optical Kerr effect (MOKE) and reflective magnetic circular dichroism (RMCD), detect changes in light polarization or reflectance induced by magnetization, providing precise magnetic ordering information [16, 17, 47, 76]. (4) Superconducting quantum interference device (SQUID) or vibrating sample magnetometer (VSM) measurements can measure magnetization intensity, but differ in their measurement accuracy. They can identify magnetic behaviors such as ferromagnetism, antiferromagnetism, and other magnetic orderings [77]. (5) Magnetic force microscopy (MFM) images magnetic domains at nanoscale resolution, allowing visualization of local magnetic properties [78]. (6) Magnetotransport measurements, particularly via the anomalous Hall effect (AHE), are highly sensitive to magnetization states and can detect complex spin textures and non-collinear antiferromagnetism [16,59]. Additional techniques include Lorentz transmission electron microscopy [79] and diamond nitrogen-vacancy (NV) center-based quantum sensing [80]. Typically, a combination of methods is required for comprehensive characterization. To facilitate a comprehensive understanding of 2D magnetism, Table 1 [12–17, 37, 40–45, 48–54, 57, 58, 60, 81–103] presents a summary of the emergent 2D magnetic materials and their intrinsic physical properties.

4 Spin-dependent quantum tunneling

2D vdW MTJs have experienced remarkably rapid development over recent years, including the achievement of a substantial TMR ratio of 340% [18]. These devices are meticulously fabricated via dry transfer techniques, where each layer is precisely assembled through mechanical exfoliation. Dry transfer offers distinct advantages over conventional magnetron sputtering: it requires only an optical imaging and alignment system, significantly simplifying the fabrication process. This technology facilitates flexible multilayer integration through van der Waals interactions, eliminating the need for lattice matching or specific substrates, while minimizing energetic particle damage—thereby preserving crystalline integrity and enhancing MTJ performance. As a result, dry transfer has become a pivotal method for constructing 2D vdW MTJs.

Among 2D ferromagnetic materials, Fe_3GeTe_2 and Fe_3GaTe_2 are extensively utilized in MTJs due to their metallic conductivity, robust ferromagnetism, and substantial PMA. Although Fe_3GaTe_2 was reported more recently (in 2022) [15] than Fe_3GeTe_2 (2018) [14], it exhibits a notably higher Curie temperature (TC) of 350–380 K, which exceeds room temperature and is substantially greater than that of Fe_3GeTe_2 (∼220 K) [14, 15]. However, the stronger interlayer vdW forces in Fe_3GaTe_2 make mechanical exfoliation more challenging compared to Fe_3GeTe_2. Therefore, both materials are promising for MTJ and other spintronic applications. Other ferromagnetic materials such as $Cr_{0.85}Te$ [104] and Cr_3Te_4 [76] are also commonly integrated into MTJs.

The tunneling barrier layer in MTJs directly affects both the tunneling resistance and the spin filtering effect, and therefore plays a critical role in determining the RA and TMR. Various 2D materials have been explored as tunnel barrier in MTJs, including semiconductors such as WS_2 [76, 105], WSe_2 [18, 106], InSe [107], MoS_2 [104], GaSe [108], $MoSe_2$ [109], $Cr_2Ge_2Te_6$ [110], as well as insulating h-BN [111, 112]. Interestingly, a magnetoresistance effect has been observed even in a Fe_3GeTe_2 bilayer homojunction without a dedicated barrier, showing a detectable resistance change between parallel and antiparallel magnetic configurations [113]. The use of various 2D barriers enables a diverse range of MTJ architectures, circumventing the lattice-matching limitations inherent in conventional CoFeB/MgO/CoFeB systems. Although 2D materials can also be integrated with traditional thin-film technologies [114, 115], this review focuses exclusively on MTJs composed entirely of 2D materials.

A typical 2D vdW MTJ is structured as a three-layer stack on a SiO_2/Si substrate, often encapsulated with a 2D insulating layer to prevent oxidation. Figure 3(a) illustrates a representative $Fe_3GaTe_2/WSe_2/Fe_3GaTe_2$ MTJ encapsulated with h-BN [116]. Variations in the thickness of Fe_3GaTe_2 flakes lead to differences in coercivity, which

Table 1 Electromagnetic characteristics of representative 2D magnetic materials.

Material	Layer number or thickness	Magnetism	Transition temperature (K)	Characterization method	Band gap (eV)	Refs.
$FePS_3$	1 L	AFM	118	Raman	1.5 (bulk)	[37]
CrI_3	1 L/bulk	FM/AFM	45/61	MOKE, RMCD	∼1.0/1.2	[12, 48–50]
$CrBr_3$	1 L	FM	27	MCD	1.38	[50, 51]
$CrCl_3$	Few layer	AFM	15	Magnetoresistance measurement	1.58 (1 L)	[50, 52]
$Cr_2Ge_2Te_6$	2 L/bulk	FM	30/68	MOKE	0.374/0.74	[13, 43, 44]
Fe_3GeTe_2	1 L/bulk	FM	20/180 130/220	Magnetotransport RMCD	Metal	[41] [14]
$MnBi_2Te_4$	7 L	FM	20	Magnetotransport	0.052	[81]
$NiPS_3$	2 L/bulk	AFM	130/155	Raman	1.4 (few layer)	[53, 54]
$FePSe_3$	3 L	AFM (bulk)	108 (bulk)	VSM	1.3 (bulk)	[57, 58]
$CrSe_2$	1 L	FM	65	RMCD	Metal	[17]
$CrTe_2$	∼11 L	FM	213	RMCD	Metal	[45]
$MnSe_2$	1 L	FM	300	SQUID	Metal	[82]
CrSBr	2 L	AFM	132	MFM	1.5	[83, 84]
NiI_2	3 L	AFM	35	Raman	1.11 (1 L)	[85, 86]
UOTe	Few layer	AFM	150	Magnetotransport	Metal	[87]
Tetragonal FeTe	∼7 L (5 nm)	AFM	45	Magnetotransport	Metal	[88]
Cr_2S_3	15 nm	AFM/FM	75/120	VSM	0.15 (few layer)	[40, 89–91]
Cr_2Te_3	5.5 nm	FM	280	Magnetotransport	Metal	[92, 93]
Cr_5Te_8	6 nm	FM	125 (tr-phase), 150 (m-phase)	Magnetotransport	Metal	[94, 95]
Cr_3Te_4	3.3 nm	FM	165	RMCD	Metal	[16, 96]
Fe_3Sn_2	8.8 nm	FM	>300	Magnetotransport	Metal	[42]
$Co_3Sn_2S_2$	35 nm	FM	175	Magnetotransport	Metal	[97]
$CoFe_2O_4$	3.8 nm	FM	>300	MFM	1.44 (bulk)	[98, 99]
$Mn_{0.14}Cr_{0.86}Te$	1.8/2.5/17.9 nm	FM	135/140/335	MOKE	Metal	[100]
Co	Nanosheets	FM	710	VSM	Metal	[101]
Fe_3O_4	13 nm	FM	>300	VSM	Metal	[102]
Fe_2O_3	18.8 nm	FM	>300	VSM	Metal	[60, 103]
Hexagonal FeTe	4 nm	FM	170	Magnetotransport	Metal	[88]
Fe_3GaTe_2	9–112 nm	FM	350–380	Magnetotransport	Metal	[15]

modify the spin-dependent transport properties. The $Fe_3GaTe_2/WSe_2/Fe_3GaTe_2$ MTJ demonstrates a substantial TMR ratio of 85% at room temperature and impressive 164% at 10 K [116]. The decrease in TMR at elevated temperatures is mainly attributed to reduced spin polarization due to thermal effects, consistent with Bloch's law: $P(T) = P(0)(1 - \alpha T^{3/2})$, where $P(0)$ is the spin polarization at 0 K, and α is a material-dependent constant [109,116,117]. The TMR ratio also exhibits voltage bias dependence in 2D MTJs featuring non-linear tunneling. This behavior is governed by underlying physical mechanisms, including bias-induced alterations in spin polarizability, the spin filtering effect, and k-space band matching, among other factors [108, 118, 119]. In addition to high TMR ratios, these devices achieve functional operation with low RA, meeting critical requirements for low-power applications [109, 117, 120]. Furthermore, using different 2D ferromagnetic materials within a single MTJ can broaden the antiparallel switching window, compensating for the limited coercivity differences due to thickness variations [120]. For a comprehensive overview, Table 2 [18, 104–112, 116–118, 120–123] summarizes key parameters and reported performance metrics of 2D vdW MTJs.

Two primary tunneling mechanisms are observed in 2D vdW MTJs, which can be distinguished through their output characteristic curves. At low bias voltages—well below the effective tunnel barrier height—direct tunneling dominates, exhibiting an approximately linear current density-voltage (J-V) relationship [108, 120]. Conversely, when the applied bias exceeds the barrier height, Fowler-Nordheim (F-N) tunneling becomes prevalent, resulting in a non-linear J-V characteristic [108, 120]. The transition between these regimes stems from the bias-induced modulation of the tunnel barrier. Under direct tunneling, the barrier shape remains largely unaffected due to the low electric field, whereas F-N tunneling involves significant barrier tilting caused by higher fields [21, 120]. The effective tunnel-barrier height itself is influenced by the material composition, thickness, and crystalline quality of the barrier layer [21, 107, 120]. Notably, the TMR ratio behaves differently in the two regimes: it remains roughly

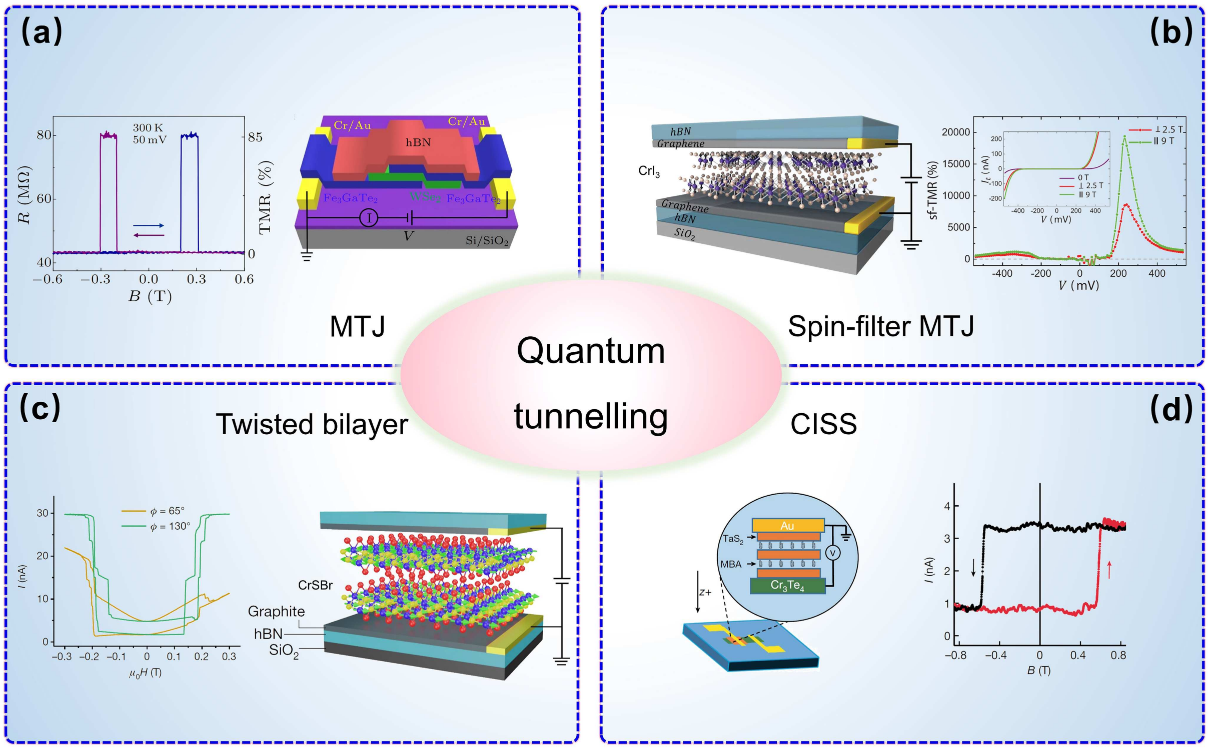

Figure 3 (Color online) Quantum tunnel effect of spin-polarized electrons. (a) Room-temperature TMR and schematic diagram of a 2D vdW $Fe_3GaTe_2/WSe_2/Fe_3GaTe_2$ MTJ [116] Copyright 2022 IOP Publishing; (b) schematic diagram and corresponding TMR of a spin-filter MTJ employing antiferromagnetic CrI_3 as a tunnel barrier [127] Copyright 2018 American Association for the Advancement of Science; (c) tunnel current and schematic diagram of a spin-filter MTJ utilizing twisted CrSBr as a tunnel barrier [130] Copyright 2024 Springer Nature; (d) schematic diagram and tunnel current behavior of CISS devices featuring a chiral-molecule-intercalated 2D TaS_2 structure acting as a tunnel barrier [134] Copyright 2022 Springer Nature.

Table 2 Summarized performance metrics for 2D vdW MTJs.

Structure	Temperature (K)	TMR (%)	RA (kΩ·μm^2)	Ref.
$Fe_3GeTe_2/WSe_2/Fe_3GeTe_2$	10	26	∼32	[106]
Fe_3GeTe_2/h-BN/Fe_3GeTe_2	4.2	160	∼76	[111]
Fe_3GaTe_2/h-BN/Fe_3GaTe_2	10 300	120 14	–	[112]
$Cr_{0.85}Te/MoS_2/Cr_{0.85}Te$	2	−7	∼4000000	[104]
$Fe_3GeTe_2/MoS_2/Fe_3GeTe_2$	10	4	28	[121]
Fe_3GeTe_2/h-BN/Fe_3GeTe_2	1.5	36 12	∼700 ∼65	[122]
$Fe_3GeTe_2/WS_2/Fe_3GeTe_2$	10	0.45	∼26	[105]
$Fe_3GaTe_2/WSe_2/Fe_3GaTe_2$	2 300	340 50	∼700 ∼1040	[18]
$Fe_3GeTe_2/InSe/Fe_3GeTe_2$	10	41 14	180 45	[107]
$Fe_3GeTe_2/GaSe/Fe_3GeTe_2$	10	192	∼800	[108]
$Fe_3GaTe_2/WSe_2/Fe_3GaTe_2$	10 300	164 85	– ∼840000	[116]
$Fe_3GaTe_2/MoSe_2/Fe_3GaTe_2$	2 300	37.7 3.7	5.2 5.6	[109]
$Fe_3GaTe_2/WS_2/Fe_3GaTe_2$	10 300	213 11	∼4000 –	[123]
$Fe_3GaTe_2/MoS_2/Fe_3GaTe_2$	2.3 300	15.9 0.3	∼13 10.3	[117]
$Fe_3GeTe_2/Cr_2Ge_2Te_6/Fe_3GeTe_2$	10	−2–2	400–1000	[110]
$Cr_3Te_4/WS_2/Fe_3GeTe_2$	3	0.3–7.2	15–2288	[120]
$Fe_3GaTe_2/GaSe/Fe_3GaTe_2$	10 300	107 25	–	[118]

constant under direct tunneling but varies substantially with current under F-N tunneling [108, 120]. Typically, the TMR ratio decreases as bias voltage increases in the F-N regime and can even become negative—where the parallel configuration exhibits higher resistance than the antiparallel one [108, 124]. These variations are often attributed to bias-induced shifts in the Fermi energy (EF), altering spin polarization and the density of spin-polarized states [18, 108, 124]. A complete explanation of negative TMR in MYJ may also involve the spin-filter effect [106].

Beyond standard ferromagnet/insulator/ferromagnet MTJs, more advanced spintronic devices leveraging spin-dependent tunneling are now being realized through vdW heterostructures. Double spin-filter MTJs, for instance, employ an insulating spin-filter layer sandwiched between two non-magnetic electrodes, enabling selective transmission of spin-polarized electrons and modulating the tunneling current [125, 126]. Their resistance state depends on the relative alignment of magnetic moments in the spin-filter barriers: low resistance in parallel and high resistance in antiparallel configuration. The inherent interlayer antiparallel spin ordering in 2D A-type antiferromagnetic insulators offers a built-in spin-filtering capability, eliminating the need for artificial stacking of multiple spin-filter layers [127]. Figure 3(b) illustrates a representative spin-filter MTJ with a graphene/CrI_3/graphene structure, where CrI_3 acts as the spin-filter barrier. In this device, the tunneling current is notably suppressed at low magnetic fields due to the inhibition of spin-conserving sequential tunneling through the antiparallel-aligned CrI_3 layers. A sharp jump in current occurs when an out-of-plane field drives the transition to parallel spin alignment. The spin-filter efficiency in CrI_3 is layer-dependent, and the tunneling current responds sensitively to magnetic configuration. The corresponding output characteristics reflect systematic dependence on the magnetic order of the CrI_3. Owing to its atomically engineered vdW interface, this device achieves a remarkable TMR ratio of up to 19000%. Similarly, other antiferromagnetic MTJs have also exhibited giant magnetoresistance, thus highlighting the reliability and burgeoning potential of spin-based electronics [52, 128, 129].

In bilayer CrI_3-based MTJs, an external magnetic field facilitates a ferromagnetic state. Upon field removal, the intrinsic antiferromagnetic ordering is restored, demonstrating volatile behavior. Nevertheless, twisting strategies applied to antiferromagnetic structures have enabled nonvolatile spin-filter MTJs, offering a viable solution [130]. As shown in Figure 3(c), a spin-filter MTJ based on twisted monolayer CrSBr homojunction between graphene electrodes exploits strong in-plane magnetocrystalline anisotropy—easy along the b-axis and hard along the a-axis even at the monolayer limit [131]. This anisotropy enables precise magnetization control in individual CrSBr monolayers. The twisted interface suppresses inherent interlayer antiferromagnetic coupling, enabling nonvolatile states in zero field. The restructured easy and hard axes indicate interlayer coupling without antiferromagnetic order, supporting coherent tunneling across the CrSBr stack and yielding a TMR ratio exceeding 700%.

The chiral-induced spin selectivity (CISS) mechanism offers an alternative route for non-volitive spin control without external magnetic fields, inspiring novel spintronic designs [132, 133]. Utilizing 2D materials as a framework for chiral molecular intercalation superlattices establishes a robust solid-state chiral architecture, suitable for exploring non-volatile spintronic devices based on CISS [134]. Figure 3(d) depicts a CISS spintronic structure where chiral-molecule-intercalated TaS_2 and ferromagnetic Cr_3Te_4 generate spin-polarized current through external field-controlled magnetization. The structure acts as a multi-tunneling junction, enhancing spin filtering via sequential spin selection through chiral molecules [135]. Thus, CISS operation relies on quantum tunneling of spin-polarized electrons through chiral molecular filters. The current switching synchronized with magnetization reversal under constant voltage confirms non-volatile behavior at zero field.

Spintronic memory uses spin as a storage medium, and its capability to generate distinguishable electronic signals enables seamless integration with semiconductor circuits. The MTJ structure enables efficient spin injection through coherent scattering of spin-polarized electrons-a process rooted in quantum tunneling at the nanoscale. Going beyond conventional MTJs, the incorporation of antiferromagnetic barriers and the CISS effect has diversified spin-tunneling device paradigms. Within these developments, 2D magnetic materials emerge as a highly promising platform due to their superior magnetic properties and enhanced tunneling efficiency resulting from reduced scattering at vdW interfaces.

5 Theoretical research of 2D MTJs

Theoretically, diverse MTJs based on layered magnetic materials have been designed. First-principles calculations predict outstanding quantum tunneling properties in such systems, including high TMR ratios and low RA. These models can be classified into two fundamental structural types. (1) Vertical MTJs (Figure 4(a)): ferromagnetic layers and tunnel barriers are integrated through vdW heterostacking, as demonstrated in the preceding sections. (2) Lateral MTJs (Figure 4(b)): magnetic electrodes and barrier material are directly bonded together via atomic

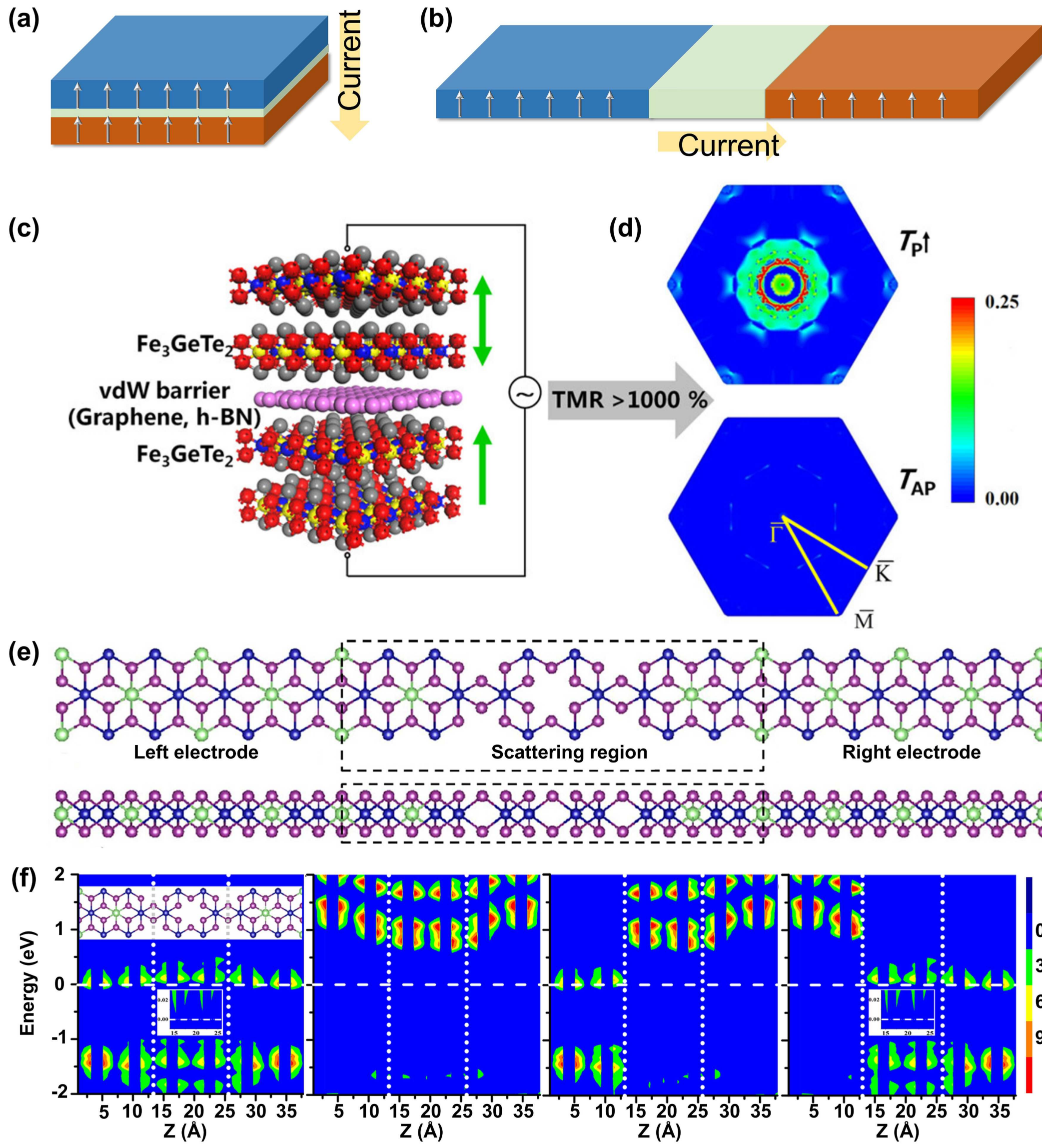

Figure 4 (Color online) Theoretical studies on MTJs. (a), (b) Schematic of vertical and lateral MTJs, respectively. (c) Structure of vdw MTJs with Fe_3GeTe_2-based electrodes, and (d) the corresponding $k_{\|}$-resolved electron transmission distribution of the Brillouin zone for parallel (top) and antiparallel spin states (bottom) [136] Copyright 2019 American Chemical Society. (e) Structure of a $Li_{0.5}CrI_3/CrI_3/Li_{0.5}CrI_3$ lateral MTJ. (f) Real-space electron density projection for the lateral MTJ. The figures from left to right are the majority and minority spin DOS for PC magnetic states, majority and minority spin DOS for APC magnetic states, respectively [140] Copyright 2020 AIP Publishing.

bonding at the interface. In this configuration, spin current tunnels directly across the barrier region, resulting in superior intrinsic performance.

Vertically stacked MTJs have become a prominent research focus in theoretical investigations owing to their structural versatility. As illustrated in Figure 4(c), the spin-dependent transport properties of a vdW MTJ incorporating a 2D Fe_3GeTe_2 electrode are presented [136]. Theoretical calculations predict that both Fe_3GeTe_2/graphene/Fe_3GeTe_2 and Fe_3GeTe_2/h-BN/Fe_3GeTe_2 vertical MTJs can achieve high TMR ratios exceeding 1000%, irrespective of the barrier material. The TMR ratio in the equilibrium state is calculated by [137]

$$\mathrm{TMR} = \frac{G_{\mathrm{PC}} - G_{\mathrm{APC}}}{G_{\mathrm{APC}}}, \tag{2}$$

where G_{PC} and G_{APC} are the total conductance for the parallel configuration (PC) and antiparallel configuration (APC) of magnetizations of Fe_3GeTe_2 electrodes, respectively. The spin-dependent conductance G of the MTJs is

Table 3 Theoretically predicted TMR in vdW MTJs.

Structure	TMR (%)	Ref.
VSe_2/MoS_2	846	[141]
Fe_3GeTe_2/graphene/Fe_3GeTe_2	3621	[136]
$Cu/CrI_3/Cu$	3000	[142]
CrI_3/h-BN/3L-CrI_3	3600	[143]
graphene/3L-CrI_3/graphene	350	[144]
$Li_{0.5}CrI_3/CrI_3/Li_{0.5}CrI_3$	1.48×10^{14}	[140]
$Fe_3GeTe_2/CrI_3/Fe_3GeTe_2$	3100	[145]
$CrTe_2$/graphene/$CrTe_2$	6962	[146]
1T-$MoSe_2$/1T-VSe_2/2H-WSe_2/1T-VSe_2/1T-$MoSe_2$	5600	[147]
graphene/bilayer $CoBr_2$/graphene	2420	[139]
graphene/bilayer $NiBr_2$/graphene	6000	[17]
graphene/trilayer $NiBr_2$/graphene	14000	
$CrSe_2/NiCl_2/CrSe_2$	5200	[148]
Au/bilayer $FeCl_2$/Au	2.7×10^3	[149]
1T-$MnSe_2$/h-BN/1T-$MnSe_2$/h-BN/1T-$MnSe_2$	2.56×10^3	[150]
$Fe_3GaTe_2/GeI_2/Fe_3GaTe_2/GeI_2/Fe_3GaTe_2$	3.61×10^9	[138]
Ag/bilayer CrOCl/Ag	48000	[86]

obtained by

$$G_\sigma = \frac{e^2}{h} \sum_{k_\parallel} T_\sigma(k_\parallel), \tag{3}$$

where e is the electron charge, h is the Planck constant, and $T_\sigma(k_\parallel)$ is the spin- and k-resolved transmission coefficient with spin σ ($\sigma = \uparrow, \downarrow$) and transverse Bloch wave vector $k_\parallel = (k_x, k_y)$ at the Fermi level.

Figure 4(d) shows the calculated spin- and $k_\parallel$-resolved transmission in Fe_3GeTe_2-based MTJs. For parallel magnetization, majority-spin transmission spans a large area of the 2D Brillouin zone (Figure 4(d), top), resembling the conducting channel distribution in the Fe_3GeTe_2 electrodes. Antiparallel magnetization shows strongly suppressed spin transmission (Figure 4(d), bottom). Since both spin and $k_\parallel$ are conserved during tunneling, transmission is much higher in parallel than antiparallel alignment, leading to high magnetoresistance in these vdW MTJs.

According to theoretical research, 2D ferromagnets contribute to fabricating MTJ with high TMR. Replacing the barrier with graphene, h-BN, or even vacuum yields similar transport behavior, indicating that the high TMR originates mainly from the spin-dependent electronic properties of the 2D Fe_3GeTe_2 electrodes [136]. However, the barrier layer influences crucial quantum tunneling phenomena, such as spin filtering and electron wave function decay, which collectively dictate spin information transfer efficiency [118, 119]. Consequently, meticulous control over the intermediate barrier material and magnetic materials is indispensable for maximizing spin polarization injection and minimizing interfacial scattering, ultimately determining the achievable TMR ratio. Additionally, high TMR can be achieved via strategic device design. Multifunctional spin diodes demonstrate high TMR, such as 3.61×10^9% and 1.02×10^6% in $Fe_3GaTe_2/GeI_2/Fe_3GaTe_2/GeI_2/Fe_3GaTe_2$ and $Fe_3GaTe_2/GeI_2/Fe_3GeTe_2/GeI_2/Fe_3GaTe_2$ [138]. Spin-filter van der Waals MTJs utilizing antiferromagnetic barriers exhibit significant TMR potential, with graphene/$CoBr_2$/graphene junctions reaching 2420% [139]; and graphite/$NiBr_2$/graphite structures with TMR achieving 6000%–14000% [17]. Table 3 [17, 86, 136, 138–150] summarizes theoretical TMR values in vdW MTJs, highlighting a promising route for high TMR using 2D intrinsic magnets.

2D lateral heterostructures establish a versatile platform for engineering novel devices with enhanced electronic functionalities. Therefore, the 2D lateral MTJs based on such heterostructures have also attracted significant theoretical interest. The $VS_2/MoS_2/VS_2$ monolayer lateral MTJ holds a giant TMR ratio of 4×10^3% and nearly 100% spin injection efficiency, both critical for high-performance spintronic devices [151]. The anisotropic MnSSe/$TaIrS_4$/MnSSe lateral MTJ integrates self-powered, near-infrared photodetection, spin valve, pure spin current, and multichannel optical communication induced by the photogalvanic effect [152]. Theoretical studies further indicate that lithium adsorption induces a transition from semiconducting to half-metallic behavior in monolayer CrI_3, which remains robust against variations in Li concentration and layer thickness [153]. Consequently, researchers designed lateral MTJs composed of a ferromagnetic CrI_3 barrier and two half-metallic $Li_{0.5}CrI_3$ electrodes, and investigated the tunnel effects using the non-equilibrium Green's function and density functional theory [140]. As illustrated in Figure 4(e), the $Li_{0.5}CrI_3/CrI_3/Li_{0.5}CrI_3$ lateral junction features a covalently bonded interface between the ferromagnetic CrI_3 barrier and the half-metallic electrodes. Owing to the half-metallicity of

Table 4 Theoretically calculated TMR in lateral MTJs.

Structure	TMR (%)	Ref.
$VS_2/MoS_2/VS_2$	4×10^3	[151]
$Li_{0.5}CrI_3/CrI_3/Li_{0.5}CrI_3$	2.86×10^{12}	[140]
$VCl_3/CoBr_3/VCl_3$	4.5×10^{12}	[159]
Bilayer $LaBr_2$	1×10^6	[154]
$VSi_2N_4/MoSi_2N_4/VSi_2N_4$	1×10^{10}	[155]
$MnGeSe_3/CrI_3/MnGeSe_3$	1×10^6	[156]
$MnSiSe_3/ZnPSe_3/MnSiSe_3$	1×10^9	[157]
Li-CrSI/CrSI/Li-CrSI	7.67×10^{14}	[158]

the $Li_{0.5}CrI_3$, the conductance in the PC exceeds that in the APC by 11 orders of magnitude, resulting in an extraordinarily high TMR of 2.68×10^{12}. This originates from the completely suppressed minority-spin channel ($0\ e^2/h$) and the dominant majority-spin channel ($1.79\ e^2/h$) in $Li_{0.5}CrI_3$, enabling highly spin-polarized transmission. Figure 4(f) shows the local DOS along the transport direction of the lateral MTJ. Insets detail the majority-spin LDOS in the CrI_3 region under PC and the minority-spin LDOS under APC near the Fermi level, confirming the preserved ferromagnetic semiconducting nature of the CrI_3 barrier. In the PC state, the majority-spin channel conducts freely with no minority-spin contribution, whereas in the APC state, both spin channels are blocked due to the antiparallel alignment, leading to drastically reduced transmission.

Lateral MTJs exhibit exceptional predicted TMR ratios due to their unique in-plane electronic transport and atomically engineered interfaces [154–158]. The absence of lattice-mismatch-induced defects at covalent interfaces sustains phase-coherent transport. Table 4 [140, 151, 154–159] summarizes theoretically predicted TMR values in lateral MTJs. Although experimental realization of these MTJs remains challenging, particularly in fabricating the ultrasmall central tunneling region, lateral MTJs hold great potential for high-performance spintronic applications.

The 2D lateral MTJs employ a planar process, which represents a significant innovation compared to the vertical process used in conventional MTJs. This structure not only simplifies the fabrication process but also enhances the stability of the device. However, the material preparation for such junctions still faces considerable challenges: firstly, the magnetic material and the middle tunnel barrier layer must achieve lattice matching to ensure a high-quality crystalline interface; secondly, the lateral dimensions of the tunnel barrier layer must be precisely controlled to below 5 nm. Addressing these challenges requires further innovation in material preparation methods.

With their exceptionally high crystallinity, 2D magnetic materials represent material systems that most closely approximate theoretical calculations. Nevertheless, the experimentally obtained TMR ratio falls considerably short of the theoretically predicted value. This discrepancy often arises from a confluence of factors, including interfacial imperfections between magnetic layers and barrier layers, magnetic domain structures, spin scattering at interfaces, and non-ideal tunneling barriers that deviate from the simplified assumptions of theoretical models. Therefore, effectively tackling these fundamental differences via optimized materials synthesis, interface engineering, and device architectures constitutes a pivotal research endeavor.

6 Future prospects

The integration of 2D magnets into MTJs heralds a transformative era for spintronics, offering capabilities far beyond those of conventional thin-film systems. However, significant challenges remain in the practical implementation of these materials into spintronic memory architectures. Despite numerous innovative concepts for novel spintronic memories utilizing 2D magnetic materials based on the quantum tunneling effect, their real-world application is hindered by issues such as high operating currents, cryogenic temperature requirements, and strong bias-voltage dependence of TMR [127, 130, 134]. As a result, advancing 2D material-based device architectures necessitates continuous research to drive the development and optimization of spin devices, including materials development, device structure design and wafer-scale fabrication technology (Figures 5(a)–(c)).

In the field of magnetic materials, there is still a severe scarcity of room-temperature 2D magnetic materials and their wafer-scale fabrication technology. To address the issue of room temperature 2D magnets, research efforts can be pursued in the following two directions. First, exploring synthesis methods for intrinsically 2D magnetic materials that exhibit room-temperature TC. Although certain metallic or semiconductor materials meet these requirements theoretically [160–171], their experimental realization has not yet been achieved (Figure 5(a)). Second, chemical doping or functionalization represents a viable approach to enhance magnetic coupling in existing 2D magnets, potentially elevating their TC to room temperature.

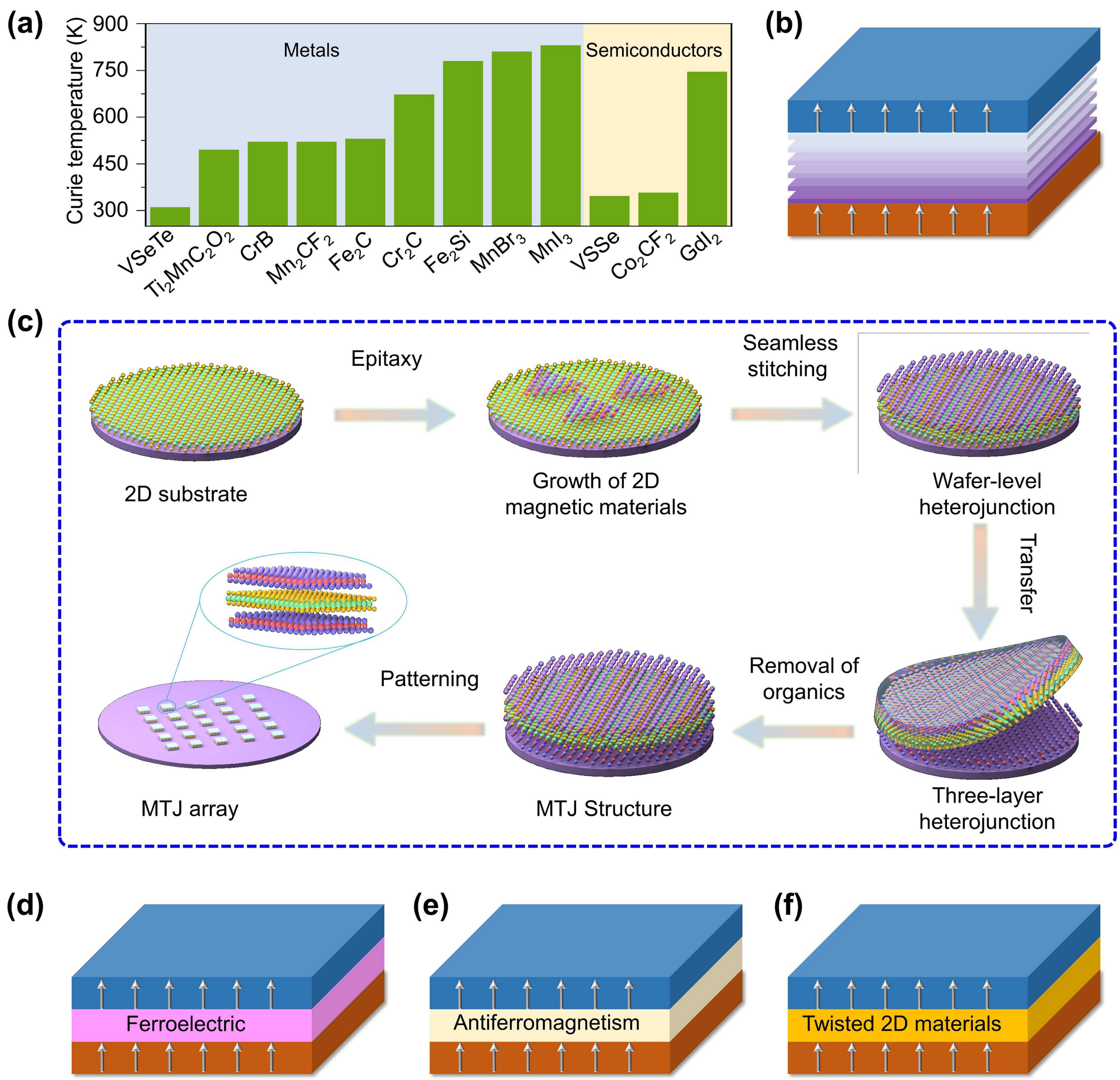

Figure 5 (Color online) Prospect of 2D materials in MTJ design. (a) Room-temperature magnetic materials predicted by theoretical calculations [160–171]; (b) advanced MTJ designs employing multi-layered stacking; (c) the fabrication strategy for MTJ arrays encompasses the preparation of wafer-scale 2D magnetic materials and subsequent multilayer heterojunctions. Exploration of a novel MTJ design leveraging (d) ferroelectric, (e) twisted 2D materials and (f) antiferromagnetic as tunneling barriers.

For practical applications, wafer-scale fabrication represents a critical challenge for 2D MTJs. A promising approach involves vapor-phase synthesis combined with a transfer process (Figure 5(c)). Owing to a preferred growth orientation for 2D magnetic materials on 2D monocrystalline substrates, the 2D nanosheets can seamlessly merge to a wafer-scale film [120]. Therefore, wafer-scale 2D heterostructures can be fabricated by epitaxially growing wafer-scale 2D room-temperature magnetic materials on 2D substrates such as MoS_2 or WS_2. Subsequently, 2D heterostructures are transferred onto another wafer-scale 2D room-temperature magnetic material to construct complete wafer-scale 2D MTJs. Finally, 2D material-based MTJ arrays can be fabricated with etching techniques compatible with semiconductor manufacturing (Figure 5(c)). During the construction of multi-layer heterogeneous structures, this dry transfer assembly technology effectively prevents direct contact between the liquid and the heterojunction interface, thereby enabling the creation of complex multi-layer stacks with clean interfaces.

In terms of device structures, Figures 3(d)–(f) present a variety of novel MTJs. However, these structures commonly suffer from a significant issue: high RA, which leads to increased power consumption in the final devices. Therefore, future research could focus on identifying materials with magnetic structures similar to CrI_3 and CrSBr, but with superior electrical conductivity, to achieve better performance balance in MTJs. Additionally, exploring highly conductive materials with helical structures—which often exhibit chirality—could enable the realization of spin-filtering devices when integrated with magnetic materials into heterostructures (Figure 5(b)). Although multiply twisted transition metal dichalcogenides (TMDs) with spiral configurations have been reported [172], further exploration is still needed to discover intrinsic chiral materials that combine high conductivity and ultrathin thickness, thereby balancing TMR and RA in MTJs. Furthermore, 2D superlattice materials—whether synthesized via intercalation [173] or occurring naturally [174]—exhibit a repeating structure of "magnetic layer/tunneling barrier/magnetic layer/tunneling barrier/...". If adjacent magnetic layers are antiferromagnetically coupled in their ground state, this coupling may transition to a ferromagnetic state under an external magnetic field. Such a structure enables repeated filtering of spin during tunneling, offering promising potential for constructing high-performance MTJs.

On the level of physical mechanisms, if the tunneling layer of a 2D MTJ is constructed from ferroelectric materials (Figure 5(d)) or twisted bilayers of TMDs (Figure 5(e)), it could potentially introduce ferroelectric polarization or valley degrees of freedom into the MTJ [175]. This would enable multi-state memory functionality and further promote innovation in tunneling physics based on the synergistic control of multiple degrees of freedom. On the other hand, if the tunneling layer is replaced with an antiferromagnetic material (Figure 5(f)), it may be possible to achieve a spin-pinning effect within a single MTJ, offering new avenues for theoretical breakthroughs in the competitive mechanisms between spin coupling and tunneling.

7 Conclusion

In conclusion, the integration of 2D magnetic materials into MTJs offers a promising yet challenging pathway toward next-generation spintronic devices. The unique properties of 2D magnets—such as high spin polarization, tunable magnetic anisotropy, and novel spin transport mechanisms—provide opportunities for significantly enhancing MTJ performance. Both theoretical and experimental advances underscore the potential of these materials for achieving higher TMR ratios and enabling precise nanoscale magnetization control. However, their practical application and commercialization face considerable obstacles, particularly in the development of room-temperature magnetic systems and the design of innovative device architectures capable of sustaining high TMR and scalability. Overcoming these challenges will require targeted research and collaboration across disciplines. Looking forward, 2D magnetic materials are expected to play a pivotal role in advancing high-performance MTJ technologies and shaping the future of spintronics.

Acknowledgements This work was supported by National Key Research and Development Program of the Ministry of Science and Technology (Grant No. 2024YFA1208401), National Natural Science Foundation of China (Grant Nos. 62322406, 62174051, 52221001), "111 Center" (Grant No. B25033), and Open Research Fund of Suzhou Laboratory (Grant No. SZLAB-1508-2024-TS013).

References

1 Incorvia J A C, Xiao T P, Zogbi N, et al. Spintronics for achieving system-level energy-efficient logic. Nat Rev Electr Eng, 2024, 1: 700–713
2 Baibich M N, Broto J M, Fert A, et al. Giant magnetoresistance of (001)Fe/(001)Cr magnetic superlattices. Phys Rev Lett, 1988, 61: 2472–2475
3 Miyazaki T, Tezuka N. Giant magnetic tunneling effect in Fe/Al_2O_3/Fe junction. J Magn Magn Mater, 1995, 139: L231–L234
4 Moodera J S, Kinder L R, Wong T M, et al. Large magnetoresistance at room temperature in ferromagnetic thin film tunnel junctions. Phys Rev Lett, 1995, 74: 3273–3276
5 Ikeda S, Hayakawa J, Ashizawa Y, et al. Tunnel magnetoresistance of 604% at 300K by suppression of Ta diffusion in CoFeB/MgO/CoFeB pseudo-spin-valves annealed at high temperature. Appl Phys Lett, 2008, 93: 082508
6 Huang Y L, Song M Y, Lee C M, et al. A 64-kilobit spin-orbit torque magnetic random-access memory based on back-end-of-line-compatible β-tungsten. Nat Electron, 2025, 8: 794–802
7 Yuasa S, Djayaprawira D D. Giant tunnel magnetoresistance in magnetic tunnel junctions with a crystalline MgO(0 0 1) barrier. J Phys D-Appl Phys, 2007, 40: R337–R354
8 Ikeda S, Miura K, Yamamoto H, et al. A perpendicular-anisotropy CoFeB-MgO magnetic tunnel junction. Nat Mater, 2010, 9: 721–724
9 Carcia P F. Perpendicular magnetic anisotropy in Pd/Co and Pt/Co thin-film layered structures. J Appl Phys, 1988, 63: 5066–5073
10 Sato N, Xue F, White R M, et al. Two-terminal spin-orbit torque magnetoresistive random access memory. Nat Electron, 2018, 1: 508–511
11 Yang H, Valenzuela S O, Chshiev M, et al. Two-dimensional materials prospects for non-volatile spintronic memories. Nature, 2022, 606: 663–673
12 Huang B, Clark G, Navarro-Moratalla E, et al. Layer-dependent ferromagnetism in a van der Waals crystal down to the monolayer limit. Nature, 2017, 546: 270–273
13 Gong C, Li L, Li Z, et al. Discovery of intrinsic ferromagnetism in two-dimensional van der Waals crystals. Nature, 2017, 546: 265–269
14 Fei Z, Huang B, Malinowski P, et al. Two-dimensional itinerant ferromagnetism in atomically thin Fe_3GeTe_2. Nat Mater, 2018, 17: 778–782
15 Zhang G, Guo F, Wu H, et al. Above-room-temperature strong intrinsic ferromagnetism in 2D van der Waals Fe_3GaTe_2 with large perpendicular magnetic anisotropy. Nat Commun, 2022, 13: 5067

16 Li B, Deng X, Shu W, et al. Air-stable ultrathin Cr_3Te_4 nanosheets with thickness-dependent magnetic biskyrmions. Mater Today, 2022, 57: 66–74
17 Guo X, Yang B, Zhang X, et al. Giant tunneling magnetoresistance induced by bias voltage in spin-filter van der Waals magnetic tunnel junctions with an interlayer antiferromagnetic semiconductor barrier. Phys Rev B, 2021, 104: 144423
18 Pan H, Singh A K, Zhang C, et al. Room-temperature tunable tunneling magnetoresistance in $Fe_3GaTe_2/WSe_2/Fe_3GaTe_2$ van der Waals heterostructures. InfoMat, 2024, 6: e12504
19 Wang X, Tang J, Xia X, et al. Current-driven magnetization switching in a van der Waals ferromagnet Fe_3GeTe_2. Sci Adv, 2019, 5: eaaw8904
20 Li W, Zhu W, Zhang G, et al. Room-temperature van der Waals ferromagnet switching by spin-orbit torques. Adv Mater, 2023, 35: 2303688
21 Simmons J G. Generalized formula for the electric tunnel effect between similar electrodes separated by a thin insulating film. J Appl Phys, 1963, 34: 1793–1803
22 Yuasa S, Hono K, Hu G, et al. Materials for spin-transfer-torque magnetoresistive random-access memory. MRS Bull, 2018, 43: 352–357
23 Butler W H, Zhang X G, Schulthess T C, et al. Spin-dependent tunneling conductance of Fe|MgO|Fe sandwiches. Phys Rev B, 2001, 63: 054416
24 Mott N F. The electrical conductivity of transition metals. Proc R Soc London Ser-Math Phys Sci, 1936, 153: 699–717
25 Yakushiji K, Noma K, Saruya T, et al. High magnetoresistance ratio and low resistance-area product in magnetic tunnel junctions with perpendicularly magnetized electrodes. Appl Phys Express, 2010, 3: 053003
26 Bhatti S, Sbiaa R, Hirohata A, et al. Spintronics based random access memory: a review. Mater Today, 2017, 20: 530–548
27 Engel B N, Akerman J, Butcher B, et al. A 4-Mb toggle MRAM based on a novel bit and switching method. IEEE Trans Magn, 2005, 41: 132–136
28 Huai Y, Albert F, Nguyen P, et al. Observation of spin-transfer switching in deep submicron-sized and low-resistance magnetic tunnel junctions. Appl Phys Lett, 2004, 84: 3118–3120
29 Liu L, Pai C F, Li Y, et al. Spin-torque switching with the giant spin Hall effect of tantalum. Science, 2012, 336: 555–558
30 Mihai Miron I, Gaudin G, Auffret S, et al. Current-driven spin torque induced by the Rashba effect in a ferromagnetic metal layer. Nat Mater, 2010, 9: 230–234
31 Nguyen V D, Rao S, Wostyn K, et al. Recent progress in spin-orbit torque magnetic random-access memory. npj Spintronics, 2024, 2: 48
32 Salahuddin S, Ni K, Datta S. The era of hyper-scaling in electronics. Nat Electron, 2018, 1: 442–450
33 Dieny B, Prejbeanu I L, Garello K, et al. Opportunities and challenges for spintronics in the microelectronics industry. Nat Electron, 2020, 3: 446–459
34 Wei S, Liao X, Wang C, et al. Emerging intrinsic magnetism in two-dimensional materials: theory and applications. 2D Mater, 2021, 8: 012005
35 Mi M, Xiao H, Yu L, et al. Two-dimensional magnetic materials for spintronic devices. Mater Today Nano, 2023, 24: 100408
36 Dang J, Wu T, Yan S, et al. Electrical switching of spin-polarized light-emitting diodes based on a 2D $CrI_3/hBN/WSe_2$ heterostructure. Nat Commun, 2024, 15: 6799
37 Lee J U, Lee S, Ryoo J H, et al. Ising-type magnetic ordering in atomically thin $FePS_3$. Nano Lett, 2016, 16: 7433–7438
38 Fujisawa Y, Pardo-Almanza M, Garland J, et al. Tailoring magnetism in self-intercalated $Cr_{1+\delta}Te_2$ epitaxial films. Phys Rev Mater, 2020, 4: 114001
39 Yang J, Zhu C, Deng Y, et al. Magnetism of two-dimensional chromium tellurides. iScience, 2023, 26: 106567
40 Zhou X, Liu C, Song L, et al. Promoting the optoelectronic and ferromagnetic properties of Cr_2S_3 nanosheets via Se doping. Sci China-Phys Mech Astron, 2022, 65: 276811
41 Deng Y, Yu Y, Song Y, et al. Gate-tunable room-temperature ferromagnetism in two-dimensional Fe_3GeTe_2. Nature, 2018, 563: 94–99
42 Zhu M, Li Q, Guo K, et al. Two-dimensional ultrathin Fe_3Sn_2 kagome metal with defect-dependent magnetic property. Nano Lett, 2024, 24: 7483–7490
43 Ji H, Stokes R A, Alegria L D, et al. A ferromagnetic insulating substrate for the epitaxial growth of topological insulators. J Appl Phys, 2013, 114: 114907
44 Ren W, Jin K, Wang J, et al. Tunable electronic structure and magnetic anisotropy in bilayer ferromagnetic semiconductor $Cr_2Ge_2Te_6$. Sci Rep, 2021, 11: 2744
45 Meng L, Zhou Z, Xu M, et al. Anomalous thickness dependence of Curie temperature in air-stable two-dimensional ferromagnetic 1T-$CrTe_2$ grown by chemical vapor deposition. Nat Commun, 2021, 12: 809
46 Casto L D, Clune A J, Yokosuk M O, et al. Strong spin-lattice coupling in $CrSiTe_3$. APL Mater, 2015, 3: 041515
47 Zhang X, Wang J, Zhu W, et al. Giant magneto-optical effect in van der Waals room-temperature ferromagnet Fe_3GaTe_2. Chin Phys Lett, 2024, 41: 067503
48 Wang H, Fan F, Zhu S, et al. Doping enhanced ferromagnetism and induced half-metallicity in CrI_3 monolayer. EPL, 2016, 114: 47001
49 McGuire M A, Dixit H, Cooper V R, et al. Coupling of crystal structure and magnetism in the layered, ferromagnetic insulator CrI_3. Chem Mater, 2015, 27: 612–620
50 Webster L, Yan J A. Strain-tunable magnetic anisotropy in monolayer $CrCl_3$, $CrBr_3$ and CrI_3. Phys Rev B, 2018, 98: 144411
51 Kim H H, Yang B, Li S, et al. Evolution of interlayer and intralayer magnetism in three atomically thin chromium trihalides. Proc Natl Acad Sci USA, 2019, 116: 11131–11136
52 Klein D R, MacNeill D, Song Q, et al. Enhancement of interlayer exchange in an ultrathin two-dimensional magnet. Nat Phys, 2019, 15: 1255–1260
53 Kim K, Lim S Y, Lee J U, et al. Suppression of magnetic ordering in XXZ-type antiferromagnetic monolayer $NiPS_3$. Nat Commun, 2019, 10: 345
54 Ho C H, Hsu T Y, Muhimmah L C. The band-edge excitons observed in few-layer $NiPS_3$. npj 2D Mater Appl, 2021, 5: 8
55 Han H, Lin H, Gan W, et al. Field-induced spin reorientation in the Néel-type antiferromagnet $MnPS_3$. Phys Rev B, 2023, 107: 075423
56 Wiedenmann A, Rossat-Mignod J, Louisy A, et al. Neutron diffraction study of the layered compounds $MnPSe_3$ and $FePSe_3$. Solid State Commun, 1981, 40: 1067–1072
57 Du K, Wang X, Liu Y, et al. Weak van der Waals stacking, wide-range band gap, and Raman study on ultrathin layers of metal phosphorus trichalcogenides. ACS Nano, 2016, 10: 1738–1743
58 Xie Q, Hu S, Hu C, et al. Identification of phonon symmetry and spin-phonon coupling in van der Waals antiferromagnetic $FePSe_3$. Appl Phys Lett, 2023, 122: 161901
59 Li B, Zhang H, Tao Q, et al. Thickness-dependent topological Hall effect in 2D Cr_5Si_3 nanosheets with noncollinear magnetic phase. Adv Mater, 2023, 35: 2210755
60 Wang Y, Wang P, Wang H, et al. Room-temperature magnetoelectric coupling in atomically thin ε-Fe_2O_3. Adv Mater, 2023, 35: 2209465
61 Kim S K, Beach G S D, Lee K J, et al. Ferrimagnetic spintronics. Nat Mater, 2022, 21: 24–34
62 Grebenchuk S, McKeever C, Grzeszczyk M, et al. Topological spin textures in an insulating van der Waals ferromagnet. Adv Mater, 2024, 36: 2311949
63 Liu C, Zhang S, Hao H, et al. Magnetic skyrmions above room temperature in a van der Waals Ferromagnet Fe_3GaTe_2. Adv Mater, 2024, 36: 2311022
64 Almeida T P, Muxworthy A R, Kovács A, et al. Direct visualization of the thermomagnetic behavior of pseudo-single-domain magnetite particles. Sci Adv, 2016, 2: e1501801

65 De Alfaro V, Fubini S, Furlan G. A new classical solution of the Yang-Mills field equations. Phys Lett B, 1976, 65: 163–166
66 Zhou Y, Li S, Liang X, et al. Topological spin textures: basic physics and devices. Adv Mater, 2025, 37: 2312935
67 Powalla L, Birch M T, Litzius K, et al. Seeding and emergence of composite skyrmions in a van der Waals magnet. Adv Mater, 2023, 35: 2208930
68 Ding B, Li Z, Xu G, et al. Observation of magnetic skyrmion bubbles in a van der Waals ferromagnet Fe_3GeTe_2. Nano Lett, 2020, 20: 868–873
69 Jiang J, Liu X, Li R, et al. Topological spin textures in a two-dimensional $MnBi_2(Se, Te)_4$ janus material. Appl Phys Lett, 2021, 119: 072401
70 Li J, Tan A, Moon K W, et al. Tailoring the topology of an artificial magnetic skyrmion. Nat Commun, 2014, 5: 4704
71 Gilbert D A, Maranville B B, Balk A L, et al. Realization of ground-state artificial skyrmion lattices at room temperature. Nat Commun, 2015, 6: 8462
72 Hou Z, Ren W, Ding B, et al. Observation of various and spontaneous magnetic skyrmionic bubbles at room temperature in a frustrated kagome magnet with uniaxial magnetic anisotropy. Adv Mater, 2017, 29: 1701144
73 Zhu Y P, Chen X, Liu X R, et al. Observation of plaid-like spin splitting in a noncoplanar antiferromagnet. Nature, 2024, 626: 523–528
74 Tian Y, Gray M J, Ji H, et al. Magneto-elastic coupling in a potential ferromagnetic 2D atomic crystal. 2D Mater, 2016, 3: 025035
75 Seyler K L, Zhong D, Klein D R, et al. Ligand-field helical luminescence in a 2D ferromagnetic insulator. Nat Phys, 2018, 14: 277–281
76 He K, Li B, Wu S, et al. Two-dimensional WTe_2/Cr_3Te_4 heterostructures with high current-induced magnetization switching ratio. Appl Phys Lett, 2025, 127: 011903
77 Cui F, He K, Wu S, et al. Stoichiometry-tunable synthesis and magnetic property exploration of two-dimensional chromium selenides. ACS Nano, 2024, 18: 6276–6285
78 Kaiser U, Schwarz A, Wiesendanger R. Magnetic exchange force microscopy with atomic resolution. Nature, 2007, 446: 522–525
79 Kao I H, Muzzio R, Zhang H, et al. Deterministic switching of a perpendicularly polarized magnet using unconventional spin-orbit torques in WTe_2. Nat Mater, 2022, 21: 1029–1034
80 Ghiasi T S, Borst M, Kurdi S, et al. Nitrogen-vacancy magnetometry of CrSBr by diamond membrane transfer. npj 2D Mater Appl, 2023, 7: 62
81 Gong Y, Guo J, Li J, et al. Experimental realization of an intrinsic magnetic topological insulator. Chin Phys Lett, 2019, 36: 076801
82 O'Hara D J, Zhu T, Trout A H, et al. Room temperature intrinsic ferromagnetism in epitaxial manganese selenide films in the monolayer limit. Nano Lett, 2018, 18: 3125–3131
83 Rizzo D J, McLeod A S, Carnahan C, et al. Visualizing atomically layered magnetism in CrSBr. Adv Mater, 2022, 34: 2201000
84 Ziebel M E, Feuer M L, Cox J, et al. CrSBr: an air-stable, two-dimensional magnetic semiconductor. Nano Lett, 2024, 24: 4319–4329
85 Liu H, Wang X, Wu J, et al. Vapor deposition of magnetic van der Waals NiI_2 crystals. ACS Nano, 2020, 14: 10544–10551
86 Yang J, Wu B, Zhao S, et al. Multistate magnetic tunnel junction based on a single two-dimensional van der Waals antiferromagnet. Phys Rev Appl, 2024, 22: 014017
87 Broyles C, Mardanya S, Liu M, et al. UOTe: kondo-interacting topological antiferromagnet in a van der Waals lattice. Adv Mater, 2024, 37: 2414966
88 Kang L, Ye C, Zhao X, et al. Phase-controllable growth of ultrathin 2D magnetic FeTe crystals. Nat Commun, 2020, 11: 3729
89 Cui F, Zhao X, Xu J, et al. Controlled growth and thickness-dependent conduction-type transition of 2D ferrimagnetic Cr_2S_3 semiconductors. Adv Mater, 2019, 32: 1905896
90 Chu J, Zhang Y, Wen Y, et al. Sub-millimeter-scale growth of one-unit-cell-thick ferrimagnetic Cr_2S_3 nanosheets. Nano Lett, 2019, 19: 2154–2161
91 Xie L, Wang J, Li J, et al. An atomically thin air-stable narrow-gap semiconductor Cr_2S_3 for broadband photodetection with high responsivity. Adv Elect Mater, 2021, 7: 2000962
92 Wen Y, Liu Z, Zhang Y, et al. Tunable room-temperature ferromagnetism in two-dimensional Cr_2Te_3. Nano Lett, 2020, 20: 3130–3139
93 Zhong Y, Peng C, Huang H, et al. From stoner to local moment magnetism in atomically thin Cr_2Te_3. Nat Commun, 2023, 14: 5340
94 Tang B, Wang X, Han M, et al. Phase engineering of Cr_5Te_8 with colossal anomalous Hall effect. Nat Electron, 2022, 5: 224–232
95 Chen C, Chen X, Wu C, et al. Air-stable 2D Cr_5Te_8 nanosheets with thickness-tunable ferromagnetism. Adv Mater, 2022, 34: 2107512
96 Yang J, Ng J W, Zhu C, et al. Chemical vapor deposition of large-area ultrathin Cr_3Te_4 nanosheets with robust ferromagnetism. 2D Mater, 2025, 12: 015002
97 Wang Q, Zeng Y, Yuan K, et al. Magnetism modulation in $Co_3Sn_2S_2$ by current-assisted domain wall motion. Nat Electron, 2023, 6: 119–125
98 Cheng R, Yin L, Wen Y, et al. Ultrathin ferrite nanosheets for room-temperature two-dimensional magnetic semiconductors. Nat Commun, 2022, 13: 5241
99 Ravindra A V, Padhan P, Prellier W. Electronic structure and optical band gap of $CoFe_2O_4$ thin films. Appl Phys Lett, 2012, 101: 161902
100 Wen Y, Liang S, Dong Z, et al. Room-temperature intrinsic ferromagnetic chromium tellurium compounds with thickness-tunable magnetic texture. Adv Mater, 2023, 35: 2209346
101 Jiang J, Cheng R, Feng W, et al. Van der Waals epitaxy growth of 2D single-element room-temperature ferromagnet. Adv Mater, 2023, 35: 2211701
102 Wang P, Ge J, Luo J, et al. Interisland-distance-mediated growth of centimeter-scale two-dimensional magnetic Fe_3O_4 arrays with unidirectional domain orientations. Nano Lett, 2023, 23: 1758–1766
103 Qin B, Saeed M Z, Li Q, et al. General low-temperature growth of two-dimensional nanosheets from layered and nonlayered materials. Nat Commun, 2023, 14: 304
104 Zhang Y, Zou K, Gao Z, et al. Large negative magnetoresistance in all-2D-materials-based spin valves. Physica Rapid Res Ltrs, 2023, 17: 2300073
105 Hu C, Yan F, Li Y, et al. Vertical WS_2 spin valve with Ohmic property based on Fe_3GeTe_2 electrodes. Chin Phys B, 2021, 30: 097505
106 Zheng Y, Ma X, Yan F, et al. Spin filtering effect in all-van der Waals heterostructures with WSe_2 barriers. npj 2D Mater Appl, 2022, 6: 62
107 Zhu W, Lin H, Yan F, et al. Large tunneling magnetoresistance in van der Waals ferromagnet/semiconductor heterojunctions. Adv Mater, 2021, 33: 2104658
108 Zhu W, Zhu Y, Zhou T, et al. Large and tunable magnetoresistance in van der Waals ferromagnet/semiconductor junctions. Nat Commun, 2023, 14: 5371
109 Yin H, Zhang P, Jin W, et al. $Fe_3GaTe_2/MoSe_2$ ferromagnet/semiconductor 2D van der Waals heterojunction for room-temperature spin-valve devices. CrystEngComm, 2023, 25: 1339–1346
110 Wang Z A, Zhang X, Zhu W, et al. Negative-to-positive tunnel magnetoresistance in van der Waals $Fe_3GeTe_2/Cr_2Ge_2Te_6/Fe_3GeTe_2$ junctions. Chin Phys Lett, 2023, 40: 077201
111 Wang Z, Sapkota D, Taniguchi T, et al. Tunneling spin valves based on Fe_3GeTe_2/hBN/Fe_3GeTe_2 van der Waals heterostructures. Nano Lett, 2018, 18: 4303–4308
112 Pan Z C, Li D, Ye X G, et al. Room-temperature orbit-transfer torque enabling van der Waals magnetoresistive memories. Sci Bull, 2023, 68: 2743–2749
113 Hu C, Zhang D, Yan F, et al. From two- to multi-state vertical spin valves without spacer layer based on Fe_3GeTe_2 van der Waals homo-junctions. Sci Bull, 2020, 65: 1072–1077
114 Iqbal M Z, Iqbal M W, Siddique S, et al. Room temperature spin valve effect in NiFe/WS_2/Co junctions. Sci Rep, 2016, 6: 21038

115 Asshoff P U, Sambricio J L, Rooney A P, et al. Magnetoresistance of vertical Co-graphene-NiFe junctions controlled by charge transfer and proximity-induced spin splitting in graphene. 2D Mater, 2017, 4: 031004
116 Zhu W, Xie S, Lin H, et al. Large room-temperature magnetoresistance in van der Waals ferromagnet/semiconductor junctions. Chin Phys Lett, 2022, 39: 128501
117 Jin W, Zhang G, Wu H, et al. Room-temperature spin-valve devices based on $Fe_3GaTe_2/MoS_2/Fe_3GaTe_2$ 2D van der Waals heterojunctions. Nanoscale, 2023, 15: 5371–5378
118 Zhu W, Wen H, Zhu S, et al. Unconventional bias-dependent tunneling magnetoresistance in van der Waals ferromagnetic/semiconductor heterojunctions. Nat Commun, 2025, 16: 9509
119 Tornos J, Gallego F, Valencia S, et al. Ferroelectric control of interface spin filtering in multiferroic tunnel junctions. Phys Rev Lett, 2019, 122: 037601
120 He K, Li B, Nie J, et al. Two-dimensional $Cr_3Te_4/WS_2/Fe_3GeTe_2/WTe_2$ magnetic memory with field-free switching and low power consumption. Adv Mater, 2025, 37: 2419939
121 Lin H, Yan F, Hu C, et al. Spin-valve effect in $Fe_3GeTe_2/MoS_2/Fe_3GeTe_2$ van der Waals heterostructures. ACS Appl Mater Interfaces, 2020, 12: 43921–43926
122 Zhou L, Huang J, Tang M, et al. Gate-tunable spin valve effect in Fe_3GeTe_2-based van der Waals heterostructures. InfoMat, 2023, 5: e12371
123 Jin W, Zhang G, Wu H, et al. Room-temperature and tunable tunneling magnetoresistance in Fe_3GaTe_2-based 2D van der Waals heterojunctions. ACS Appl Mater Interfaces, 2023, 15: 36519–36526
124 Min K H, Lee D H, Choi S J, et al. Tunable spin injection and detection across a van der Waals interface. Nat Mater, 2022, 21: 1144–1149
125 Worledge D C, Geballe T H. Magnetoresistive double spin filter tunnel junction. J Appl Phys, 2000, 88: 5277–5279
126 Miao G X, Müller M, Moodera J S. Magnetoresistance in double spin filter tunnel junctions with nonmagnetic electrodes and its unconventional bias dependence. Phys Rev Lett, 2009, 102: 076601
127 Song T, Cai X, Tu M W Y, et al. Giant tunneling magnetoresistance in spin-filter van der Waals heterostructures. Science, 2018, 360: 1214–1218
128 Wang Z, Gutiérrez-Lezama I, Ubrig N, et al. Very large tunneling magnetoresistance in layered magnetic semiconductor CrI_3. Nat Commun, 2018, 9: 2516
129 Klein D R, MacNeill D, Lado J L, et al. Probing magnetism in 2D van der Waals crystalline insulators via electron tunneling. Science, 2018, 360: 1218–1222
130 Chen Y, Samanta K, Shahed N A, et al. Twist-assisted all-antiferromagnetic tunnel junction in the atomic limit. Nature, 2024, 632: 1045–1051
131 Telford E J, Dismukes A H, Dudley R L, et al. Coupling between magnetic order and charge transport in a two-dimensional magnetic semiconductor. Nat Mater, 2022, 21: 754–760
132 Naaman R, Waldeck D H. Spintronics and chirality: spin selectivity in electron transport through chiral molecules. Annu Rev Phys Chem, 2015, 66: 263–281
133 Dalum S, Hedegård P. Theory of chiral induced spin selectivity. Nano Lett, 2019, 19: 5253–5259
134 Qian Q, Ren H, Zhou J, et al. Chiral molecular intercalation superlattices. Nature, 2022, 606: 902–908
135 Göhler B, Hamelbeck V, Markus T Z, et al. Spin selectivity in electron transmission through self-assembled monolayers of double-stranded DNA. Science, 2011, 331: 894–897
136 Li X, Lü J T, Zhang J, et al. Spin-dependent transport in van der Waals magnetic tunnel junctions with Fe_3GeTe_2 Electrodes. Nano Lett, 2019, 19: 5133–5139
137 Yuasa S, Nagahama T, Fukushima A, et al. Giant room-temperature magnetoresistance in single-crystal Fe/MgO/Fe magnetic tunnel junctions. Nat Mater, 2004, 3: 868–871
138 Zhu Y, Guo X Y, Chi B Y, et al. Reconfigurable spin tunneling diode and giant tunneling magnetoresistance in a symmetric van der Waals double-barrier magnetic tunnel junction. Phys Rev B, 2024, 110: 054409
139 Zhu Y, Guo X Y, Jiang L N, et al. Giant tunneling magnetoresistance in van der Waals magnetic tunnel junctions formed by interlayer antiferromagnetic bilayer $CoBr_2$. Phys Rev B, 2021, 103: 134437
140 Li F, Yang B, Zhu Y, et al. Ultrahigh tunneling magnetoresistance in van der Waals and lateral magnetic tunnel junctions formed by intrinsic ferromagnets $Li_{0.5}CrI_3$ and CrI_3. Appl Phys Lett, 2020, 117: 022412
141 Zhou J, Qiao J, Duan C G, et al. Large tunneling magnetoresistance in VSe_2/MoS_2 magnetic tunnel junction. ACS Appl Mater Interfaces, 2019, 11: 17647–17653
142 Paudel T R, Tsymbal E Y. Spin filtering in CrI_3 tunnel junctions. ACS Appl Mater Interfaces, 2019, 11: 15781–15787
143 Yan Z, Zhang R, Dong X, et al. Significant tunneling magnetoresistance and excellent spin filtering effect in CrI_3-based van der Waals magnetic tunnel junctions. Phys Chem Chem Phys, 2020, 22: 14773–14780
144 Heath J J, Costa M, Buongiorno-Nardelli M, et al. Role of quantum confinement and interlayer coupling in CrI_3-graphene magnetic tunnel junctions. Phys Rev B, 2020, 101: 195439
145 Zhang X, Yang B, Guo X, et al. Ferromagnetic barrier induced large enhancement of tunneling magnetoresistance in van der Waals perpendicular magnetic tunnel junctions. Nanoscale, 2021, 13: 19993–20001
146 Zhou H, Zhang Y, Zhao W. Tunable tunneling magnetoresistance in van der Waals magnetic tunnel junctions with 1 T-$CrTe_2$ electrodes. ACS Appl Mater Interfaces, 2021, 13: 1214–1221
147 Yang W, Cao Y, Han J, et al. Spin-filter induced large magnetoresistance in 2D van der Waals magnetic tunnel junctions. Nanoscale, 2021, 13: 862–868
148 Guo X, Zhu Y, Yang B, et al. Large tunneling magnetoresistance and low resistance-area product in $CrSe_2/NiCl_2/CrSe_2$ van der Waals magnetic tunnel junction. Appl Phys Lett, 2022, 121: 042404
149 Han J, Lv C, Yang W, et al. Large tunneling magnetoresistance in van der Waals magnetic tunnel junctions based on $FeCl_2$ films with interlayer antiferromagnetic couplings. Nanoscale, 2023, 15: 2067–2078
150 Chen Z, Liu X, Li X, et al. Large tunneling magnetoresistance in spin-filtering 1T-$MnSe_2$/h-BN van der Waals magnetic tunnel junction. Nanoscale, 2023, 15: 8447–8455
151 Zhao P, Li J, Jin H, et al. Designing lateral spintronic devices with giant tunnel magnetoresistance and perfect spin injection efficiency based on transition metal dichalcogenides. Phys Chem Chem Phys, 2018, 20: 10286–10291
152 Xu D, Tan J, Ge M, et al. Multifunctional near-infrared polarized photodetector driven by the anisotropic photogalvanic effect in a two-dimensional $MnSSe/TaIrS_4/MnSSe$ magnetic tunnel junction. Phys Rev Appl, 2024, 22: 054042
153 Guo Y, Yuan S, Wang B, et al. Half-metallicity and enhanced ferromagnetism in Li-adsorbed ultrathin chromium triiodide. J Mater Chem C, 2018, 6: 5716–5720
154 Chen Q, Zheng X, Jiang P, et al. Electric field induced tunable half-metallicity in an A-type antiferromagnetic bilayer $LaBr_2$. Phys Rev B, 2022, 106: 245423
155 Wu Q, Ang L K. Giant tunneling magnetoresistance in atomically thin $VSi_2N_4/MoSi_2N_4/VSi_2N_4$ magnetic tunnel junction. Appl Phys Lett, 2022, 120: 022401
156 Song Y, Chai C, Fan Q, et al. Lateral magnetic tunnel junctions with a heterointerface-induced half-metallic electrode. J Phys Chem Solids, 2022, 167: 110754
157 Tan J, Yang G, Ouyang G. Large tunneling magnetoresistance and its high bias stability in Weyl half-semimetal based lateral magnetic tunnel junctions. New J Phys, 2024, 26: 033047

158 Li Q Q, Duan Z F, Liu W W, et al. Two-dimensional lateral magnetic tunnel junction with ultrahigh tunneling magnetoresistance. Nano Res, 2025, 18: 94907188
159 Feng Y, Wu X, Gao G. High tunnel magnetoresistance based on 2D Dirac spin gapless semiconductor VCl_3. Appl Phys Lett, 2020, 116: 022402
160 Huang C, Zhou J, Sun H, et al. Toward room-temperature electrical control of magnetic order in multiferroic van der Waals materials. Nano Lett, 2022, 22: 5191–5197
161 Sun Q, Fu Z, Yang Z. Tunable magnetic and electronic properties of the Cr-based MXene (Cr_2C) with functional groups and doping. J Magn Magn Mater, 2020, 514: 167141
162 Dou M, Li H, Yao Q, et al. Room-temperature ferromagnetism in two-dimensional transition metal borides: a first-principles investigation. Phys Chem Chem Phys, 2021, 23: 10615–10620
163 Hu Y, Liu X Y, Shen Z H, et al. High Curie temperature and carrier mobility of novel Fe, Co and Ni carbide MXenes. Nanoscale, 2020, 12: 11627–11637
164 Sun Y, Zhuo Z, Wu X, et al. Room-temperature ferromagnetism in two-dimensional Fe_2Si nanosheet with enhanced spin-polarization ratio. Nano Lett, 2017, 17: 2771–2777
165 Wang B, Zhang X, Zhang Y, et al. Prediction of a two-dimensional high- TC f-electron ferromagnetic semiconductor. Mater Horiz, 2020, 7: 1623–1630
166 He J, Lyu P, Nachtigall P. New two-dimensional Mn-based MXenes with room-temperature ferromagnetism and half-metallicity. J Mater Chem C, 2016, 4: 11143–11149
167 Sun Q, Kioussis N. Prediction of manganese trihalides as two-dimensional Dirac half-metals. Phys Rev B, 2018, 97: 094408
168 Xing S, Zhou J, Zhang X, et al. Theory, properties and engineering of 2D magnetic materials. Prog Mater Sci, 2023, 132: 101036
169 Wang M-C, Huang C-C, Cheung C-H, et al. Prospects and opportunities of 2D van der Waals magnetic systems. Annalen der Physik, 2020, 532: 1900452
170 Dong L, Kumar H, Anasori B, et al. Rational design of two-dimensional metallic and semiconducting spintronic materials based on ordered double-transition-metal MXenes. J Phys Chem Lett, 2017, 8: 422–428
171 Yue Y, Wang B, Miao N, et al. Tuning the magnetic properties of Zr_2N MXene by biaxial strain. Ceramics Int, 2021, 47: 2367–2373
172 Ji Z, Zhao Y, Chen Y, et al. Opto-twistronic hall effect in a three-dimensional spiral lattice. Nature, 2024, 634: 69–73
173 Zhou J, Zhou J, Wan Z, et al. A cation-exchange approach to tunable magnetic intercalation superlattices. Nature, 2025, 643: 683–690
174 Ng N, McQueen T M. Misfit layered compounds: unique, tunable heterostructured materials with untapped properties. APL Mater, 2022, 10: 100901
175 Eom J, Lee I H, Kee J Y, et al. Voltage control of magnetism in $Fe_{3-x}GeTe_2/In_2Se_3$ van der Waals ferromagnetic/ferroelectric heterostructures. Nat Commun, 2023, 14: 5605